Article:

Santamaria, Laura; Arregi, Aitor;; Lopez, Gartzen; Artetxe, Maite; Amutio, Maider; Bilbao, Javier; Olazar, Martin**. Effect of La2O3 promotion on a Ni/Al2O3 catalyst for H2 production in the inline biomass pyrolysis-reforming.** Fuel Volume 262, 15 February 2020, 116593

Received 4 September 2019; Received in revised form 17 October 2019; Accepted 5 November 2019. Available online 19 November 2019

https://doi.org/10.1016/j.fuel.2019.116593

Effect of La_2O_3 promotion on a Ni/Al_2O_3 catalyst for H_2 production in the in-line biomass pyrolysis-reforming

Laura Santamaria[a], Aitor Arregi[a], Gartzen Lopez[a,b]*, Maite Artetxe[a], Maider Amutio[a], Javier Bilbao[a] and Martin Olazar[a]

[a]Department of Chemical Engineering, University of the Basque Country UPV/EHU, P.O. Box 644 - E48080 Bilbao (Spain). gartzen.lopez@ehu.eus

[b]IKERBASQUE, Basque Foundation for Science, Bilbao, Spain

Abstract

The effect of La_2O_3 addition on a Ni/Al_2O_3 catalyst has been studied in the biomass pyrolysis and in-line catalytic steam reforming process. The results obtained using homemade catalysts (Ni/Al_2O_3 and Ni/La_2O_3-Al_2O_3) have been compared with those obtained using a commercial Ni reforming catalyst (G90LDP). The pyrolysis step has been performed in a conical spouted bed reactor at 500 ºC and the reforming one in a fluidized bed reactor placed in line at 600 ºC, using a space time of 20 $g_{catalyst}$ min $g_{volatiles}^{-1}$ and a steam/biomass ratio of 4. The Ni/La_2O_3-Al_2O_3 catalyst had a better performance and higher stability than G90LDP and Ni/Al_2O_3 catalysts, with conversion and H_2 yield being higher than 97 and 90 %, respectively, for more than 90 min on stream. Nevertheless, conversion and H_2 yield decreased significantly with time on stream due to catalyst deactivation. Thus, the deactivated catalysts have been characterized by N_2 adsorption-desorption, X-ray diffraction (XRD), temperature programmed oxidation (TPO), scanning electron microscopy (SEM) and transmission electron microscopy (TEM). Coke deposition has been determined to be the main cause of catalyst deactivation, with the structure of the coke being fully amorphous in the three catalysts studied.

Keywords: hydrogen, pyrolysis, reforming, biomass, Ni/Al_2O_3 catalyst, La_2O_3 promoter

1. Introduction

The use of hydrogen as a clean energy carrier, fuel and raw material for chemical synthesis is gaining increasing attention in recent years. Nevertheless, hydrogen is currently produced by reforming and gasification processes based on non-renewable sources, such as natural gas (48 %), heavy oils and naphtha (30 %) and coal (18 %) [1]. The production of hydrogen from these sources involves environmental issues related to the emission of greenhouse gases into the atmosphere, which approximately account for 500 megatonnes of CO_2 each year [2]. Consequently, renewable sources are an alternative to produce chemicals and fuels, and therefore contribute to decreasing the dependency on fossil fuels [3].

Lignocellulosic biomass is a raw material with a promising role as a renewable source for fuel and chemical production [4,5]. Biomass resources are the best alternative to fossil fuels, which can be converted into products with low carbon emissions [6,7]. Moreover, its high energy potential and availability makes biomass one of the most interesting renewable sources [8]. Amongst the thermochemical strategies to transform biomass into hydrogen or hydrogen-rich syngas, biomass gasification and the indirect bio-oil reforming route are the most studied ones [9-13].

Nevertheless, the tar obtained in the biomass gasification processes, which is a complex mixture of polycyclic aromatic compounds (larger molecules than benzene), leads to fouling of downstream equipment [14], and is therefore one of the major drawbacks of this strategy, which has not been yet solved. Tar concentration must be reduced to below 5 mg/Nm^3 for gas turbines, 1 mg/Nm^3 for methanol synthesis and 0.1 mg/Nm^3 for Fischer-Tropsch synthesis [15,16]. Regarding the indirect route based on reforming the bio-oil rather than the biomass, the higher energy density of the bio-oil compared to biomass is an important advantage to be considered, as transportation costs can be decreased by carrying out biomass pyrolysis in different geographical zones and valorising the bio-oil afterwards in centralized large scale catalytic conversion units [17]. However, problems related to raw bio-oil feeding and the losses of raw material in the bio-oil condensation and volatilization steps are the main challenges to overcome.

In this scenario, the pyrolysis and subsequent in-line catalytic steam reforming strategy is gaining increasing attention as an alternative way to biomass gasification and bio-oil reforming for H_2 production from biomass [18-22]. Amongst the different catalysts used in the biomass pyrolysis-reforming process, those based on Ni, Co and Fe are the most

used ones due to their low cost compared to noble metals [23-26]. Regarding catalyst supports, a considerable range has been reported in the literature in order to improve hydrogen production and catalyst stability [27]. Thus, conventional metal oxide supports, such us Al_2O_3, MgO, SiO_2, TiO_2 or CeO_2, have been extensively analyzed in the steam reforming of the volatiles derived from biomass pyrolysis [28,29]. Moreover, the use of alternatives supports, such as olivine [30], limonite [31], silica based materials like SBA-15, MCM-41 [32,33] or carbon based supports [34-37], are gaining increasing attention due to their lower cost. Yang et al. [38] investigated the production of H_2 in the catalytic reforming of corncob pyrolysis volatiles using Ni, Co and Ni-Co based catalysts supported on acid washed Shengly lignite (AWSL), and attained the highest H_2 production (7.26 wt. %) when they used the bimetallic catalyst. Ye et al. [39] obtained a H_2 production of 4.3 wt % using a Ni catalyst supported on MCM-41 in the pyrolysis-gasification of biomass. Waheed and Williams [40] reported a good performance of a Ni-dolomite catalyst, obtaining a maximum H_2 production of 6.1 wt %, when rice husk was valorised. Nevertheless, Al_2O_3 support is the most used in the literature in the pyrolysis and in-line reforming of biomass [41-44]. Furthermore, different promoters, such as Ca, Mg, La or Ce, have also been studied in oxygenate reforming processes. Thus, the incorporation of metal oxide promoters may positively influence both the performance and the stability of the catalyst, and also the coke formation in the reforming of biomass pyrolysis volatile compounds [45,46]. Thus, a suitable promoter may enhance the following properties: i) mechanical properties, i.e., higher mechanical strength, and therefore higher resistance to attrition, which is essential in fluidized bed reactors, ii) physical properties, which ease a better Ni dispersion, and therefore hinder deactivation by metal sintering, as well as improve the accessibility of bio-oil molecules, avoid porous structure blockage and ease regeneration by coke combustion, iii) reducibility of metallic species, since less Ni active phase on the catalysts involves faster catalyst deactivation, iv) metallic properties, namely, metal-support interaction (promotes catalyst stability), activity for in-situ coke gasification, acidity (favors coke formation and condensation) and basicity (hinders coke formation). Garcia et al. [47] reported that the addition of promoters, such as Mg and La, enhance steam adsorption in the reforming of bio-oil, which ease the gasification of the coke. Medrano et al. [48] investigated different Ni-Al catalysts modified with Ca and Mg in the reforming of the bio-oil aqueous fraction, and the Ni-

Mg-Al catalyst showed the highest conversion and H_2 concentration, with the values being 81.01 % and 63.13 vol %, respectively.

Nevertheless, although several Ni promoted catalysts have been developed and studied in the steam reforming of oxygenates (either model compounds or the aqueous fraction of bio-oil), aspects related to the performance of Ni/La_2O_3-Al_2O_3 catalysts in the two-step process of biomass pyrolysis and in-line steam reforming of the volatiles have not been reported in the literature.

Previous studies by our research group compared five supports (Al_2O_3, SiO_2, MgO, TiO_2 and ZrO_2) in the pyrolysis and in-line reforming of biomass in a conical spouted bed-fluidized bed reactor configuration, with the best results of hydrogen production and catalyst stability being obtained when Al_2O_3, MgO and ZrO_2 were used [49-51]. In order to improve catalyst's performance and stability, this study aimed at promoting the Ni/Al_2O_3 catalyst with La_2O_3 promoter. The influence of La_2O_3 addition on the conversion, product yields and catalyst deactivation has been studied in-depth. Moreover, the fresh and deactivated catalysts have been characterized in order to study the cause and effect of catalyst deactivation.

2. Experimental

2.1. Biomass properties

Pine wood waste *(pinus insignis)* is the biomass used in this process, with the particle size ranging between 1 and 2 mm. The ultimate and proximate analyses have been determined in previous studies [52,53] and the main results are summarized in Table 1. The higher heating value (HHV) is 19.8 MJ kg^{-1}, which has been measured by a *Parr 1356* isoperibolic bomb calorimeter.

Table 1. Pine wood sawdust characterization.

Ultimate analysis (wt %)	
Carbon	49.33
Hydrogen	6.06
Nitrogen	0.04
Oxygen	44.57
Proximate analysis (wt %)	
Volatile matter	73.4
Fixed carbon	16.7
Ash	0.5
Moisture	9.4
HHV (MJ kg^{-1})	19.8

2.2. Catalysts

2.2.1. Catalyst synthesis

Two catalysts (Ni/Al_2O_3 and Ni/La_2O_3-Al_2O_3) were synthesized for this study. The homemade catalysts were also compared with a commercial Ni reforming one (G90LDP), which is used in industry for CH_4 reforming. All catalysts have been sieved to a particle size in the 0.4-0.8 mm range in order to obtain a suitable fluidization regime [53].

Prior to catalyst synthesis, γ-Al_2O_3 was pretreated by calcination under air atmosphere at 1000 ºC for 5 h in order to thermally stabilize the support, avoiding therefore any possible phase change of Al_2O_3 during the process, as well as improving catalyst's mechanical strength. It is to note that the complete transformation of γ-Al_2O_3 into α-Al_2O_3 is achieved at temperatures above 1100-1200 ºC [54,55], and the commercial Al_2O_3 support used in this study contains a small amount of SiO_2, which shifts the phase transition towards higher temperatures [56,57]. Thus, the features of the Al_2O_3 support will be similar to those of the bare γ-Al_2O_3.

The Ni/Al_2O_3 catalyst was prepared by wet impregnation of the support with an aqueous solution of $Ni(NO_3)_2 \cdot 6H_2O$ *(VWR Chemicals, 99 %)*. After the impregnation, the catalyst was dried at 100 ºC for 24 h, followed by a calcination step at 700 ºC for 3 h.

The modified support was prepared by a subsequent wet impregnation method. Prior to Ni loading, the Al_2O_3 was modified with the promoter oxide (La_2O_3) by impregnating it with an aqueous solution of $La(NO_3)_3 \cdot 6H_2O$ *(VWR Chemicals, 99 %)*. The concentration of the metal-promoter oxide was fixed at 10 wt % La_2O_3 on Al_2O_3. The support was dried overnight and calcined at 900 ºC for 3 h. Subsequently, Ni was loaded by impregnating the support with a metal precursor ($Ni(NO_3)_2 \cdot 6H_2O$), drying at 100 ºC overnight and calcining at 700 ºC for 3 h. A nominal content of 10 wt % was the target.

2.2.2. Catalyst characterization

The specific surface area and the properties of the porous structure (average pore size and pore volume) of the catalysts were determined by N_2 adsorption-desorption in a *Micromeritics ASAP 2010* apparatus. The experimental procedure consisted in degasifying the sample at 150 ºC for 8 h to remove any impurity in the sample, followed by an adsorption-desorption of N_2 (99.9995 % purity) in multiple equilibrium stages until saturation of the sample at cryogenic temperature (liquid N_2) was attained.

X-ray fluorescence (XRF) spectrometry was used to measure the total metal loading (wt %) in each catalyst. The chemical analysis was carried out under vacuum atmosphere using a sequential wavelength dispersion X-ray fluorescence spectrometer, *PANalytical AXIOS*, equipped with a Rh tube and three detectors (gaseous flow, scintillation and Xe sealing).

The temperature programmed reduction (TPR) of the catalysts consisted in exposing the solid to a reducing gas flow, while a linear temperature sequence was maintained. The reduction rate was determined by measuring continuously the H_2 consumed, which allowed knowing the reduction temperature of the different metallic phases in the catalyst. This analysis was carried out in a *Micromeritics AutoChem 2920*, where a flow of 10 vol % H_2/Ar circulated through the sample. Then, the sample was heated from room temperature to 900 ºC, with a constant heating rate of 5 ºC min^{-1}.

X-ray powder diffraction (XRD) patterns were recorded in a *Bruker D8 Advance* diffractrometer with a $CuK_{\alpha 1}$ radiation in order to analyse the crystalline structure of the calcined and reduced catalysts. The average Ni crystallite size was calculated by using the Scherrer formula. The device is equipped with a Germanium primary monochromator, Bragg-Brentano geometry and with a $CuK_{\alpha 1}$ wavelength of 1.5406 (Å), corresponding to an X-ray tube with Cu anticathode. Sol-X dispersive energy detector was employed, with a window optimized for $CuK_{\alpha 1}$ for limiting the fluorescence radiation. Data collection was carried out continuously, from 10º to 80º, with steps of 0.04º in 2θ, and measurement times per step of 12 s.

Furthermore, the amount of coke deposited on the deactivated catalysts was determined by means of air combustion in a *TA Instruments TGA Q5000* thermogravimetric (TG) apparatus, coupled in-line with a *Balzers Instruments Thermostar* mass spectrometer (MS), which recorded the signals at 14, 18, 28 and 44 atomic numbers, corresponding to N_2, H_2O, CO and CO_2, respectively. However, the coke content has been determined based on the CO_2 signal, as the H_2O formed during combustion and that corresponding to the moisture cannot be distinguished and, furthermore CO is immediately oxidized to CO_2 activated by the metallic function of the catalyst. The following procedure was carried out: stripping with N_2 (10 mL min^{-1}) at 100 ºC to remove the impurities, and heating with air (50 mL min^{-1}) to 800 ºC by following a 5 ºC min^{-1} ramp, with that temperature being kept for 30 min for obtaining full coke combustion.

In addition, the nature and location of the coke on the catalyst were also studied by scanning electron microscopy (SEM) images (*JEOL JSM-6400*) and transmission electron microscopy (TEM) images (*Philips CM200*).

2.3. Equipment and reactors

The general scheme of the bench scale plant used in the pyrolysis-reforming process is shown in Figure 1. The reaction system is equipped with two in-line reactors: (i) a conical spouted bed reactor (CSBR) for biomass pyrolysis and (ii) a fluidized bed reactor (FBR) for the reforming of pyrolysis volatiles. A detailed description of the reactors has been reported elsewhere [49,58,59]. The reactors are located inside a forced convection oven, which consists of two heating cartridges of 1500 W and two centrifugal fans to induce forced convection in order to maintain the box temperature at

300 ºC, and therefore avoid the condensation of heavy oxygenate compounds. Moreover, the CSBR has a lateral outlet pipe placed above the bed surface for the removal of char particles from the bed.

The bench scale plant is equipped with feeding devices for solid, water and gas. The biomass feeding system consists of a cylindrical vessel equipped with a vertical shaft connected to a piston placed below the material bed. By ascending the piston, the biomass falls into the reactor through a tube cooled with tap water. A *Gilson 307* pump supplies water to the reactor, which, prior to entering the gas preheater, is vaporized in a heating cartridge located inside the hot box. Different gases (N_2, air and H_2) can also be fed into the lower part of the pyrolysis reactor.

Moreover, the product separation system consists of a solid-gas separation system provided with a cyclone and a filter, and a liquid-gas separation system consisting of a condenser and a coalescence filter.

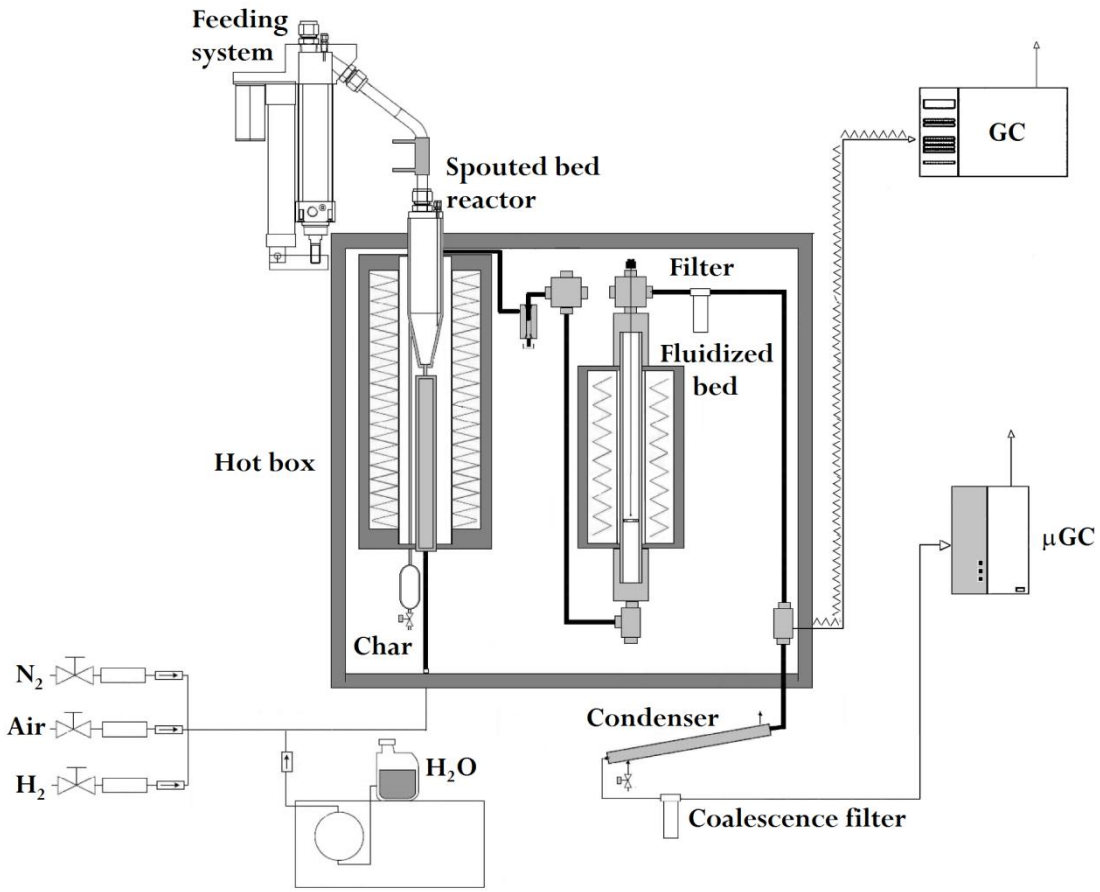

Figure 1. Scheme of the bench scale pyrolysis-reforming plant.

2.4. Experimental conditions

The pyrolysis step was carried out at 500 ºC, which was set as the most suitable temperature based on the previous experiments performed by the research group [52,53]. Thus, 0.75 g min^{-1} of biomass were continuously fed into the pyrolysis and in-line reforming unit. Furthermore, the steam flow rate and particle size of the sand in the CSBR are conditioned by the hydrodynamic requirements of the CSBR. Based on these requirements, a water flow rate of 3 mL min^{-1} was established as suitable, which corresponds to a steam flow of 3.73 NL min^{-1}. In order to achieve high turbulence in the bed, 30 g of sand were used with a size in the 0.30-0.35 mm range.

Once hydrodynamic runs were carried out in the FBR at the reforming temperature (600 ºC) with the bed amount of 25 g, particle sizes in the 0.4-0.8 mm and 0.30-0.35 mm ranges were selected for the catalyst and sand, respectively, as the most suitable ones.

The experiments performed with different catalysts were carried out with a space time of 20 g_{cat} min $g_{volatiles}^{-1}$ and a steam/biomass ratio (S/B) of 4. These conditions were previously determined as the optimum ones in the pyrolysis and in-line reforming of pine sawdust [53,59].

2.5. Product analysis

The analysis of the products was out in-line using a gas chromatograph for volatile products (GC *Varian 3900*) and gas micro-chromatograph for permanent gases (micro GC *Varian 4900*). The gas chromatograph (*Varian 3900*) is equipped with a HP-Pona column and a flame ionization detector (FID). Samples were injected into the gas chromatograph by means of a line thermostated at 280 ºC, with reproducibility being ensured by several replicates under the same conditions. The gas micro-chromatograph (*Varian 4900*) has four different channels with four analytical modules, including injector, columns and detector. This micro-chromatograph was used to quantify the concentration of non-condensable gases, with the sampling point being placed downstream the devices for condensing and filtering the gas.

2.6. Reaction indices

In order to quantify the process results, conversion and individual product yields have been defined. Conversion has been determined as the ratio between the moles of C

recovered in the gaseous product (F_{gas}) and those fed into the reforming step ($F_{volatiles}$), without considering the C contained in the char, which is taken out from the CSBR and is not therefore reformed.

$$X = \frac{F_{gas}}{F_{volatiles}} \cdot 100 \quad (1)$$

Similarly, the yield of each C containing individual compound has been calculated based on the volatiles derived from biomass pyrolysis, where F_i and $F_{volatiles}$ are the molar flow rates of product i and pyrolysis volatile stream, respectively, given in C units contained.

$$Y_i = \frac{F_i}{F_{volatiles}} \cdot 100 \quad (2)$$

The H_2 yield is defined based on the maximum allowable by stoichiometry (eq. (3)), where F_{H2} and F_{H2}^0 are the actual H_2 molar flow rate and the maximum allowed by stoichiometry, respectively.

$$C_nH_mO_k + (2n-k)H_2O \rightarrow nCO_2 + (2n+m/2-k)H_2 \quad (3)$$

$$Y_{H_2} = \frac{F_{H_2}}{F_{H_2}^{\ 0}} \cdot 100 \quad (4)$$

Finally, H_2 production (eq. (5)) is defined by mass unit of the biomass in the feed, where m_{H2} and m_0 are the mass flow rates of the H_2 produced and biomass fed into the process, respectively.

$$P_{H_2} = \frac{m_{H_2}}{m_0} \cdot 100 \quad (5)$$

3. Results

3.1. Fresh catalyst characterization

The textural properties of the calcined catalysts were studied by the N_2 adsorption-desorption technique. Table 2 shows the BET surface area, pore volume and pore

diameter of the catalysts. The BET surface area of the commercial Ni reforming catalyst (G90LDP) [53,60] is especially low, whereas those of the homemade Ni/Al_2O_3 and Ni/La_2O_3-Al_2O_3 catalysts are significantly higher. Nevertheless, when the Ni metal phase and the La_2O_3 promoter are added to the Al_2O_3 support, the surface area decreases, as Ni and La_2O_3 particles are deposited on the pores of the support, and N_2 cannot therefore access to the pores [19]. Some authors reported that there is no interaction between the support and the promoter for La_2O_3 loadings above 5 wt %, thus levelling off the decreasing trend in surface area [61,62]. In addition, pore volume remains almost constant when La_2O_3 is impregnated. Regarding average pore diameter, it increases slightly after the Ni impregnation step, given that the finest pores are partially blocked by Ni sites. Furthermore, in the case of Ni/La_2O_3-Al_2O_3 catalyst, the average pore diameter increases considerably due to the higher volume of La_2O_3 molecule in relation to Ni particle, and therefore micropores undergo blockage [63]. Navarro et al. [64] also reported a decrease in the catalyst surface, an increase in the average pore size and no impact on the pore volume when incorporating La_2O_3 in the Ni/La_2O_3-Al_2O_3 catalyst.

The metallic properties (Ni content, particle diameter and dispersion) of the commercial and homemade catalysts are shown in Table 2. As observed, the Ni content of the calcined catalysts measured by XRF spectrometry are close to the nominal Ni loading of 10 wt %. This result implies that, although the Ni content in the catalysts modified with La_2O_3 is slightly lower than the nominal one, the impregnation method carried out in this study is suitable for catalyst synthesis. The Ni/Al_2O_3 catalyst has the highest Ni dispersion, which is explained by its high specific surface area [65,66].

Table 2. Physical and metallic properties of the catalysts.

Catalyst	Physical properties			Metallic properties		
	S_{BET} ($m^2\ g^{-1}$)	V_{pore} ($cm^3\ g^{-1}$)	d_{pore} (Å)	Ni content (wt %)	d_M[a] (nm)	Ni dispersion[b] (%)
G90LDP	19	0.04	122	11.3	24	4
Al_2O_3	87	0.38	173	-	-	-
Ni/Al_2O_3	76	0.39	182	9.8	10	9.7
Ni/La_2O_3-Al_2O_3	52	0.39	214	8.1	20	4.9

288 [a] *Calculated from the full width at half the maximum of the Ni (2 0 0) diffraction peak at 2θ= 52° in the*
289 *XRD using the Scherrer equation.*

290 [b] *Dispersion calculated by (97.1 nm)/(Particle size of Ni (nm)) [67].*

291 Figure 2 shows the TPR profiles of G90LDP, Ni/Al_2O_3 and Ni/La_2O_3-Al_2O_3 catalysts.
292 The TPR profile of the G90LDP commercial catalyst shows a main peak at around 550
293 ºC, which is attributable to the reduction of NiO interacting with the α-Al_2O_3 support,
294 and another peak at 700 ºC, corresponding to the spinel $NiAl_2O_4$. In the case of
295 Ni/Al_2O_3 and Ni/La_2O_3-Al_2O_3, the peak located at around 450 ºC is attributable to the
296 reduction of NiO, which is weakly interacting with the support [49,68], whereas the
297 peaks in the 600-700 ºC range are attributed to the reduction of dispersed NiO species,
298 which interact strongly with the Al_2O_3 support [64]. Moreover, the peaks observed
299 above 700 ºC are due to the Ni particles that have migrated into the Al_2O_3 support to
300 form $NiAl_2O_4$, which is resistant to reduction and stable even at 900 ºC [69]. The
301 addition of La_2O_3 promoter to the Ni/Al_2O_3 catalyst increases the reduction capacity of
302 NiO species strongly interacting with the support (peak at around 700 ºC). A decrease in
303 the $NiAl_2O_4$ phase is also observed in the Ni/La_2O_3-Al_2O_3 catalyst, thereby improving
304 the reducibility of the Ni/Al_2O_3 catalyst.

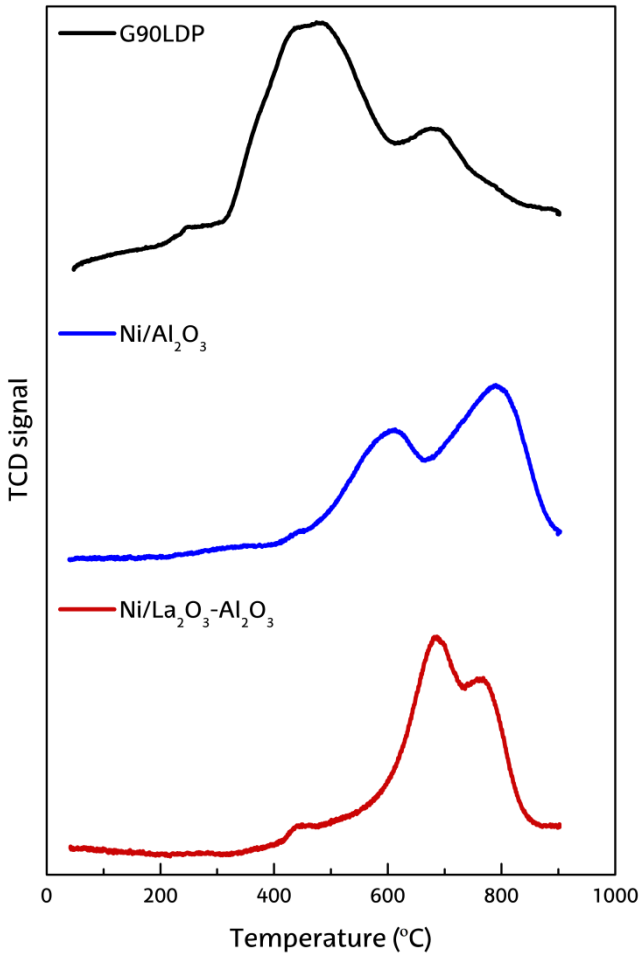

305

306 **Figure 2.** Temperature programmed reduction (TPR) profiles of Ni based fresh
307 catalysts.

308 Several phases may be identified in the XRD diffractogram of reduced catalysts (Figure
309 3), as are those corresponding to Ni, Al_2O_3 and calcium aluminate phases ($CaO(Al_2O_3)_2$,
310 $CaAl_2O_4$, $CaAl_{12}O_{19}$). The catalysts exhibit diffraction lines at 2θ= 44º, 52º and 76º,
311 ascribed to crystalline phases of Ni corresponding to the planes (1 1 1), (2 0 0) and (2 2
312 0), respectively [70,71]. Although the $NiAl_2O_4$ phase is difficult to observe in the XRD
313 profiles, 2θ= 29º, 45º and 60º are probably associated with this spinel [69], which
314 overlap those corresponding to Al_2O_3 phase.

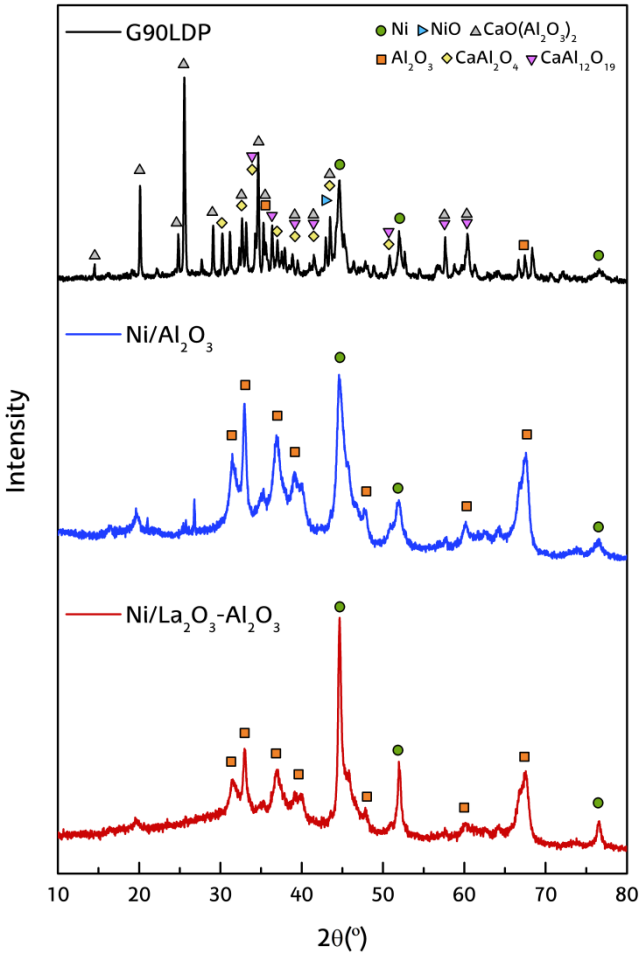

Figure 3. X-ray diffraction (XRD) profiles of Ni based reduced catalysts.

It should be noted that the La species (La_2O_3, $LaAlO_3$...) in the Ni/La_2O_3-Al_2O_3 catalyst are not identified in the XRD diffractogram, which is explained by the low crystallinity, addition of a low amount of La_2O_3 or small particle sizes [72,73]. Yamamoto et al. [74] concluded that even for loadings above 25 wt % La_2O_3, La species cannot be detected using the XRD technique. Moreover, La species are deposited on the alumina in a very dispersed way or forming a two-dimensional layer of lanthanum oxide [75,76]. Furthermore, based on the results obtained by XRD, Ni crystallite size in the different catalysts has been calculated applying the equation by Debye-Scherrer to $2\theta = 52^\circ$ diffraction bands. Thus, as observed in Table 2, the size of Ni crystallite decreases as follows: G90LDP > Ni/La_2O_3-Al_2O_3 > Ni/Al_2O_3. The G90LDP catalyst has the highest Ni crystallite size values followed by Ni/La_2O_3-Al_2O_3, which is related to the low surface area of these catalysts. Thus, irrespective of other catalyst features, a low specific surface area would lead to a poorer active phase dispersion, thereby resulting in

higher Ni particle sizes. Moreover, as observed in Table 2, the dispersion values are rather low, especially when La_2O_3 is added to the Al_2O_3 support, presumably due to the low surface area of the support and high Ni loadings [77].

3.2. Conversion and product yields

A study has been carried out of the effect the performance of different catalysts has on the reforming step of biomass pyrolysis volatiles and, particularly, on conversion and product yields, with their evolution with time on stream being conditioned by catalyst deactivation. Previous studies report the insignificant effect of using steam in the biomass pyrolysis step [49,53], which is due to the relative low pyrolysis temperature (500 ºC) and low residence time of the volatiles in the CSBR. Similarly, Mellin et al. [78] confirmed the inert nature of steam in the pyrolysis of biomass, as they obtain negligible differences in terms of heat transfer and product formation rates when N_2 and steam were fed into the pyrolysis reactor. This strategy of using steam for pyrolysis eases the configuration of the process, given that no separation of the inert gas from the product stream is required and water is easily condensed. Thus, the product stream obtained in the pyrolysis step is summarized in Table 3, with the gas and bio-oil fractions being subsequently fed into the second reforming step. A detailed description of the main products obtained in the pyrolysis step can be found elsewhere [49,53].

Table 3. Product distribution in the steam pyrolysis of biomass at 500 ºC.

Compound	Yield (wt %)
Gas	**7.3**
CO	3.38
CO_2	3.27
Hydrocarbons (C_1-C_4)	0.68
Bio-oil	**75.3**
Acids	2.73
Aldehydes	1.93
Alcohols	2.00
Ketones	6.37
Phenols	16.49
Furans	3.32
Saccharides	4.46
Water	25.36
Char	**17.3**

In order to ascertain the behaviour of the commercial and homemade catalysts, and compare their catalytic performance, the following reactions have been considered:

Steam reforming of oxygenate compounds:

$$C_nH_mO_k + (n-k)H_2O \rightarrow nCO + (n+m/2-k)H_2 \quad (6)$$

Water gas shift (WGS) reaction:

$$CO + H_2O \leftrightarrow CO_2 + H_2 \quad (7)$$

CH_4 steam reforming:

$$CH_4 + H_2O \leftrightarrow CO + 3H_2 \quad (8)$$

C_2-C_4 hydrocarbons steam reforming:

$$C_nH_m + nH_2O \rightarrow nCO + (n+m/2)H_2 \quad (9)$$

Cracking of oxygenate compounds (secondary reaction):

$$C_nH_mO_k \rightarrow C_xH_yO_z + C_aH_b + CH_4 + CO + CO_2 + C \quad (10)$$

Figure 4 shows the evolution of conversion with time on stream for G90LDP, Ni/Al_2O_3 and Ni/La_2O_3-Al_2O_3 catalysts. As observed, conversion at zero time on stream is almost full and similar for the three catalysts studied, with the values being 99.7, 98.4 and 99.6 % for G90LDP, Ni/Al_2O_3 and Ni/La_2O_3-Al_2O_3 catalysts, respectively, i.e., the volatiles derived from biomass pyrolysis are almost completely reformed. When the G90LDP catalyst is used, conversion decreases sharply with time on stream above 75 min, with the value being 57.2 % subsequent to 105 min on stream. This decrease is attributable to the non-reformed oxygenate compounds, which are assumed to be the main coke precursors [53,59]. The homemade Ni/Al_2O_3 catalyst has a better performance than the commercial one, with conversion being 73.9 % subsequent to 103 min on stream, i.e., conversion is approximately 17 % higher when the homemade catalyst is used instead of the commercial one for a time on stream slightly above 100 min. Nevertheless, the commercial catalyst shows better performance for the first 60 min on stream, as conversion is almost constant, whereas in the case of the Ni/Al_2O_3 catalyst it decreases

subsequent to the initial 20-30 min operation. Although the G90LDP catalyst has lower BET surface area and lower Ni dispersion than the Ni/Al_2O_3 one, Ni is located on the external surface of the support in the former, improving therefore the accessibility of the reactants to Ni active sites. In addition, the trend observed for the G90LDP catalyst is explained by its content of Ca, which reduces the acidity of the Al_2O_3 support, thus hindering cracking reactions, and therefore decreasing coke formation [79]. The higher stability of the G90LDP catalyst in the first minutes is also related to the higher Ni content of this catalyst (11.3 wt %) compared to the Ni/Al_2O_3 (9.8 wt %) (see Table 2).

In order to improve catalytic performance, the Ni/Al_2O_3 catalyst has been promoted by adding La_2O_3. As observed in Figure 4, the conversion is similar to the commercial one for the first 75 min on stream, but it improves significantly above this time on stream, with the value being 96.4 % subsequent to 108 min on stream (39.2 % higher than that of the commercial one) and decreasing to 63.8 % subsequent to 206 min on stream. This trend is explained by the basic character of La_2O_3 promoter, which reduces the acidity of the support and inhibits the formation of coke [72]. Moreover, La_2O_3 promoter favours water adsorption and dissociation, thus gasifying the coke deposited and preventing catalyst deactivation [47,80].

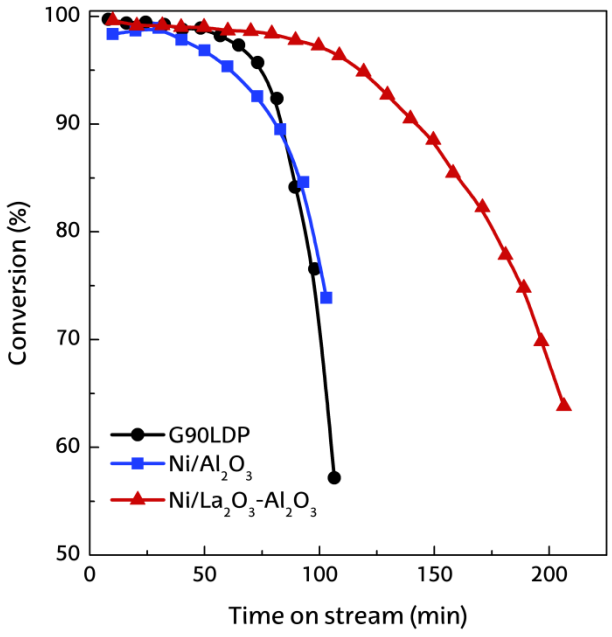

Figure 4. Evolution of conversion with time on stream. Reforming conditions: 600 ºC; space time, 20 g_{cat} min $g_{volatiles}^{-1}$; S/B ratio, 4.

Figure 5 shows the evolution of the yields of H_2 (Figure 5a), CO_2 (Figure 5b), CO (Figure 5c), CH_4 (Figure 5d), C_2-C_4 hydrocarbons (Figure 5e) and non-converted oxygenates (Figure 5f) with time on stream. As observed in Figure 5a, H_2 yield at zero time on stream is similar for all the catalysts studied (≈ 93 %), and the evolution with time on stream follows a similar trend as conversion. The H_2 yield decreases with time on stream, due to the decrease in activity for reforming and WGS reactions [48,81]. When G90LDP and homemade Ni/Al_2O_3 catalysts are used, H_2 yield values are similar due to their similar composition, whereas the Ni/La_2O_3-Al_2O_3 catalyst shows higher activity and H_2 yield, which is maintained above 90 % for around 90 min on stream. These results are consistent with those reported in the steam reforming of the aqueous fraction of bio-oil [82] and raw bio-oil [83], in which the La_2O_3 promoted catalyst has a good performance in terms of H_2 activity and stability. However, as mentioned before, no study has been reported in the literature concerning the use of this Ni/La_2O_3-Al_2O_3 catalyst in the biomass pyrolysis-reforming process. It is to note that the highest H_2 production by mass unit is obtained when G90LDP catalyst is used (11.2 wt %), followed by Ni/Al_2O_3 (10.1 wt %) and Ni/La_2O_3-Al_2O_3 (10.0 wt %), which is explained by the higher Ni content of the commercial catalyst, especially in the case of Ni/La_2O_3-Al_2O_3. Bizkarra et al. [73] also reported faster deactivation of the Ni/Al_2O_3 catalyst, as it does not prevent carbon deposition on the catalyst surface.

Similarly, CO_2 yield also decreases with time on stream, showing a similar trend as H_2 yield. Regarding by-products yields, those of CO, CH_4, C_2-C_4 hydrocarbons and non-converted oxygenate compounds increase with time on stream due to the decrease in the activity of the catalyst for reforming and WGS reactions, and therefore higher extent of secondary cracking reactions [84-86]. It should be remarked the higher initial yield of CO_2 and lower initial yield of CO obtained when the Ni/Al_2O_3 catalyst is used, which is explained by its higher Ni content than the Ni/La_2O_3-Al_2O_3 catalyst and, especially, its higher Ni particle dispersion than Ni/La_2O_3-Al_2O_3 and commercial G90LDP catalysts. In addition, the lowest CH_4 yield at zero time on stream is also obtained with the Ni/Al_2O_3 catalyst due to the aforementioned properties of this catalyst.

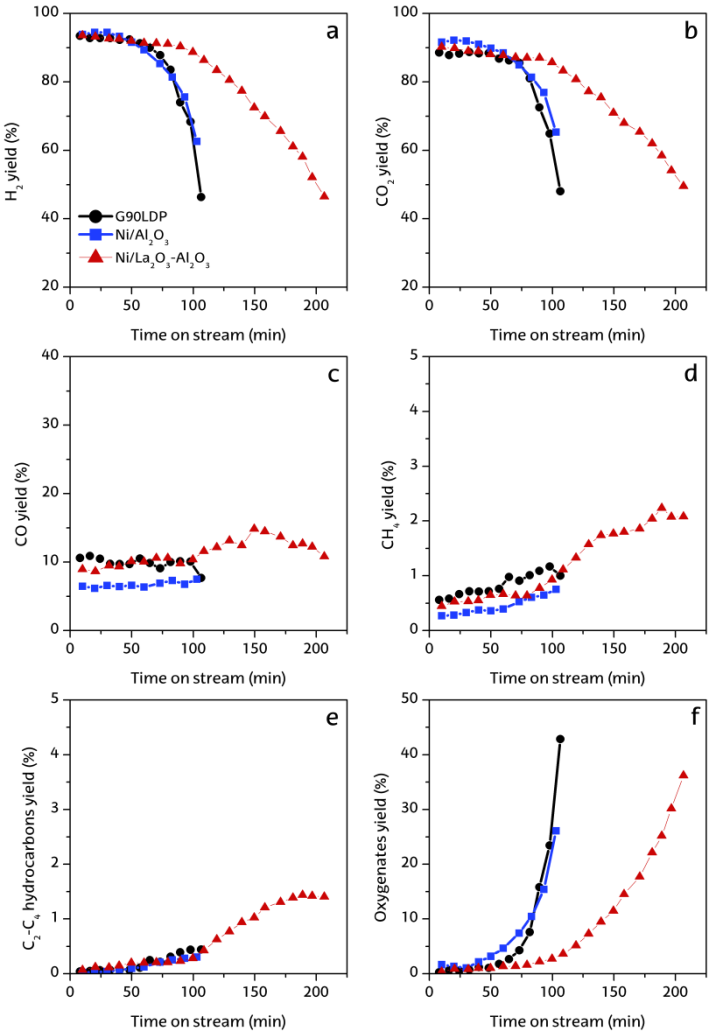

425

426 **Figure 5.** Evolution of product yields with time on stream: H_2 (a), CO_2 (b), CO (c),
427 CH_4 (d), C_2-C_4 hydrocarbons (e) and oxygenate compounds (f). Reforming
428 conditions: 600 ºC; space time, 20 g_{cat} min $g_{volatiles}^{-1}$; S/B ratio, 4.

429 3.3. Catalyst deactivation

430 Previous studies by the research group reported Ni sintering and, especially, coke
431 deposition as the main causes of catalyst deactivation in the reforming of biomass
432 pyrolysis volatiles [59,87]. Table 4 shows the physical properties of the fresh and
433 deactivated catalysts in order to compare the changes produced by coke deposition in
434 the textural properties of the catalysts. In the case of the commercial catalyst (G90LDP),
435 the results indicate that coke deposition partially blocks the porous structure of the
436 catalyst, as the average pore size increases considerably from 122 to 243 Å because
437 blockage by coke affects certain mesopores and, especially, micropores [87]. Moreover,

pore volume is not significantly affected by the coke deposition on the catalyst. Furthermore, the Ni/Al_2O_3 and Ni/La_2O_3-Al_2O_3 catalysts have smaller pore volume and mean pore diameter when the catalysts are deactivated, which is explained by the partial blockage of the pores due to coke deposition, especially the biggest ones [49]. Regarding BET surface areas, they are almost similar for all the catalyst studied, with no meaningful differences between fresh and deactivated catalysts, which is evidence that the pores are partially blocked, but they are all accessible.

Table 4. Physical properties of the fresh and deactivated catalysts.

Catalyst	S_{BET} (m^2 g^{-1})		V_{pore} (cm^3 g^{-1})		d_{pore} (Å)	
	Fresh	**Deact.**	**Fresh**	**Deact.**	**Fresh**	**Deact.**
G90LDP	19	17	0.11	0.10	122	243
Ni/Al_2O_3	76	75	0.39	0.29	182	153
Ni/La_2O_3-Al_2O_3	52	53	0.39	0.21	214	156

The deterioration with time on stream of the metallic properties of the catalysts has been studied by analyzing the Ni crystallite size of the fresh and deactivated catalysts, which have been calculated applying the equation by Debye-Scherrer to the $2\theta = 52^\circ$ diffraction bands obtained from the XRD difractograms shown in Figures 3 and 6 for the fresh and deactivated catalysts, respectively. No significant differences are observed in the case of Ni/Al_2O_3 catalyst when the reduced and deactivated XRD profiles are compared. Navarro et al. [64] also reported similar diffraction peaks as those obtained for the reduced catalysts in the steam reforming of acetone, with no structural modifications being observed after the reforming reaction. However, the XRD profiles of the Ni/La_2O_3-Al_2O_3 catalyst shows some structural changes, as the characteristic diffraction peaks at 27º, 33º, 37º and 39º related to La_2O_3 species come out after operation at reaction conditions. The fact that this species did not appear in the reduced XRD profile is due to the initial low particle size of the La_2O_3 crystallites, which undergo a substantial growth after the reforming reaction, and are therefore visible by XRD technique. Furthermore, Table 5 shows the average Ni crystallite size of the fresh and deactivated catalysts. As observed, the Ni crystallite size of the deactivated G90LDP catalyst increased considerably, from 25 nm in the fresh catalyst to 39 nm in the deactivated one. Nevertheless, previous studies have proven that Ni particle reaches a steady size after 100 min on stream [87]. In the case of the homemade Ni/Al_2O_3 and

466 Ni/La_2O_3-Al_2O_3 catalysts, the differences in Ni crystallite size between fresh and
467 deactivated catalysts are not significant, with the increase being from 10 to 13 nm for
468 the Ni/Al_2O_3 catalyst and from 20 to 24 nm for the Ni/La_2O_3-Al_2O_3 catalyst. Thus, Ni
469 sintering is not the main cause of the fast deactivation observed for these catalysts.

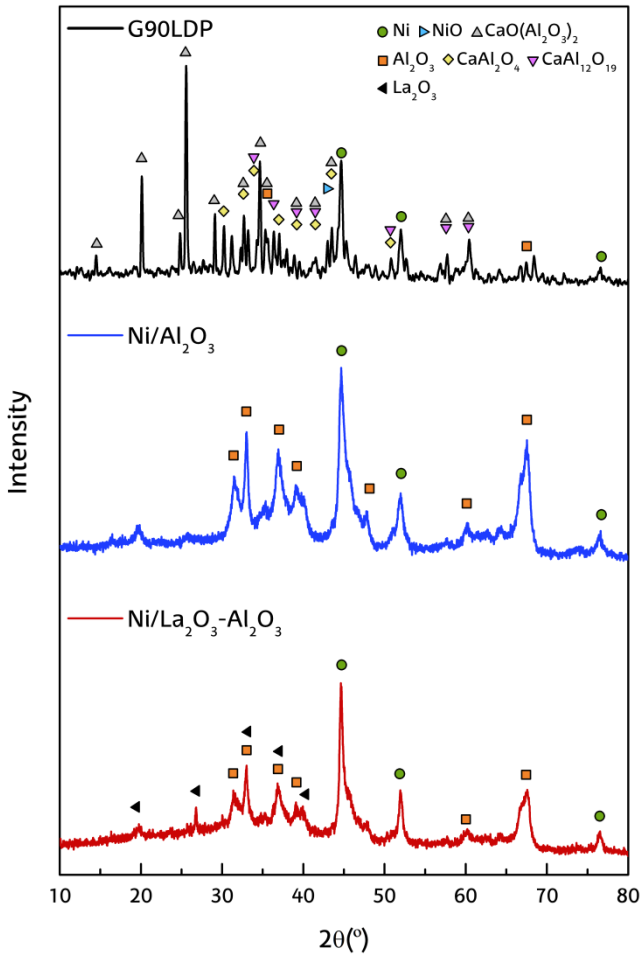

470

471 **Figure 6.** X-ray diffraction (XRD) profiles of deactivated catalysts.

472 Nevertheless, the main deactivating cause of the reforming catalysts is related to coke
473 deposition [59,87-89]. Figure 7 displays the TPO profiles obtained with the commercial
474 G90LDP and the homemade deactivated catalysts. As observed, two main peaks are
475 observed in the three catalysts studied, which correspond to cokes of different location
476 and/or composition. In the case of G90LDP catalyst, the first peak is located in the 420-
477 430 ºC range and is related to the coke deposited on Ni particles (encapsulating the
478 active sites of the catalyst), whereas the second peak (in the 520-565 ºC range)

corresponds to the coke located further from these sites and is burnt at higher temperatures due to its more structured nature [59,87]. Similarly, two types of coke can also be distinguished in the Ni/Al_2O_3 catalyst, whose combustion peaks are located at temperatures of around 480 and 600 ºC. Initially the coke precursors are deposited on Ni active sites, promoted by the acid sites of the Al_2O_3 support, which afterwards migrate towards the support [50,90,91]. Finally, the two types of coke observed for the Ni/La_2O_3-Al_2O_3 catalyst burn at lower temperatures compared to G90LDP and Ni/Al_2O_3 catalysts by the promotion of La_2O_3, which inhibits coke evolution due to its basicity and water adsorption capacity during the reforming reaction [92,93].

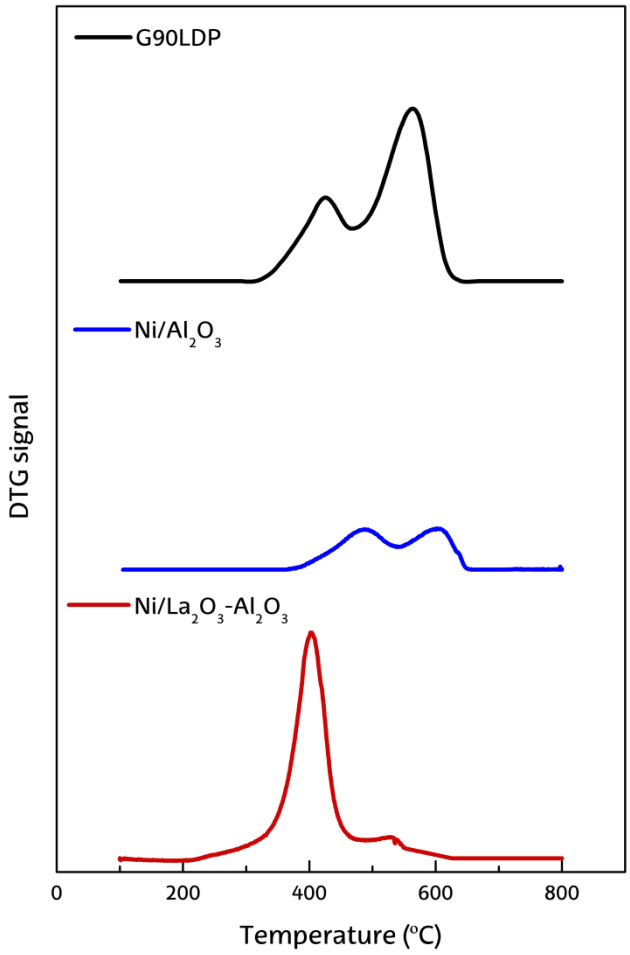

Figure 7. Temperature programmed oxidation (TPO) profiles of Ni based deactivated catalysts.

Given that reaction time is different in each experiment, the amount of coke deposited per biomass mass unit has been calculated based on the TPO results shown above. Thus, the values of coke content (C_C), reaction time and average coke deposition rate (r_C) are shown in Table 5. The coke deposition rate on the catalysts decreases as follows: G90LDP > Ni/La_2O_3-Al_2O_3 ≈ Ni/Al_2O_3. As observed, the highest coke deposition rate is observed when the commercial G90LDP catalyst is used, which is specifically designed for CH_4 reforming and is considerably deactivated when oxygenated compounds are fed. Accordingly, the comparison between the commercial and the prepared Ni/Al2O3 catalysts revealed that the coke deposited on the commercial catalyst for a similar reaction time (100 min on stream) is more than 3 times the one measured in the synthesized catalyst. The coke deposition rate is considerably reduced using Ni/Al_2O_3 and Ni/La_2O_3-Al_2O_3 catalysts. The good performance of the Ni/La_2O_3-Al_2O_3 catalyst has been proven, which is explained by the capability of La_2O_3 promoter for adsorbing H_2O, thus maintaining the catalyst activity. Nevertheless, a higher amount of coke has been deposited on the Ni/La_2O_3-Al_2O_3 catalyst than on the Ni/Al_2O_3 one after the reforming reaction, with the average coke deposition rate being slightly higher. This result is a consequence of the stronger reaction conditions, given that the Ni/La_2O_3-Al_2O_3 catalyst has been exposed to higher partial pressures of non-converted oxygenate compounds, and therefore the extension of coke formation is higher.

Based on these results, there is no direct relationship between the deactivation and coke content and coke formation rate, which reveals a more complex dependency of the latter on deactivation, which in turn depends on the initial activity of the catalyst and the nature and location of the coke deposited.

Table 5. Values of Ni particle diameter, total coke content and the average coke deposition rate for different catalysts.

Catalyst	Metallic properties		Coke deposition		
	d_{Ni}[a] (nm)		C_C	Time on	r_C
	Fresh	Deact.	(wt %)	stream (min)	($mg_{coke}\ g_{cat}^{-1}\ g_{biomass}^{-1}$)
G90LDP	24	43	9.90	106	1.25
Ni/Al_2O_3	10	13	2.84	103	0.37
Ni/La_2O_3-αAl_2O_3	20	24	6.84	206	0.44

[a] *Calculated from the full width at half maximum of the Ni (2 0 0) diffraction peak at 2θ= 52 º in the XRD using the Scherrer equation.*

In order to analyze the coke nature, Figure 8 shows the SEM images of the deactivated G90LDP, Ni/Al_2O_3 and Ni/La_2O_3-Al_2O_3 catalysts. As observed, all the samples show an amorphous coke layer on the catalyst surface, with no filamentous coke being observed, i.e., although coke undergoes graphitization, filaments are not formed. Moreover, the coke deposited on all the deactivated catalysts is non-uniformly distributed. Unfortunately, it is not easy to distinguishing the different metal oxides from the Ni active phase, as they have a similar atomic number, which hinders contrast in the SEM images. These results are in-line with the profiles obtained in the TPO analyses.

In order to complete the information about the morphology of the coke deposited on the catalysts, Figure 9 shows the TEM images of the deactivated G90LDP, Ni/Al_2O_3 and Ni/La_2O_3-Al_2O_3 catalysts. The bigger Ni crystallite size calculated by XRD profiles in the G90LDP catalyst is confirmed by the TEM images. Furthermore, only amorphous coke is observed in the images, without any specific morphology, although the condensation degree and location differ in the catalysts. Thus, the features of Ni/La_2O_3-Al_2O_3 catalyst (basicity and water adsorption) lead to a higher stability, minimizing coke deposition and enhancing precursor gasification [77,94].

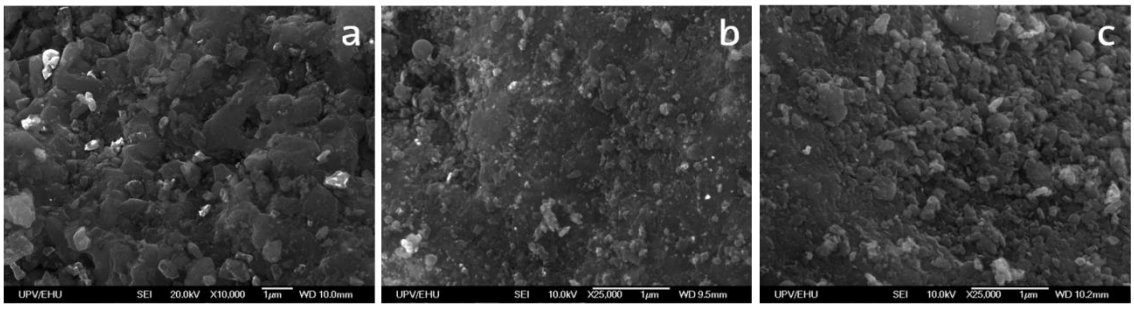

Figure 8. SEM images of the deactivated catalysts: G90LDP (a), Ni/Al_2O_3 (b) and Ni/La_2O_3-Al_2O_3 (c).

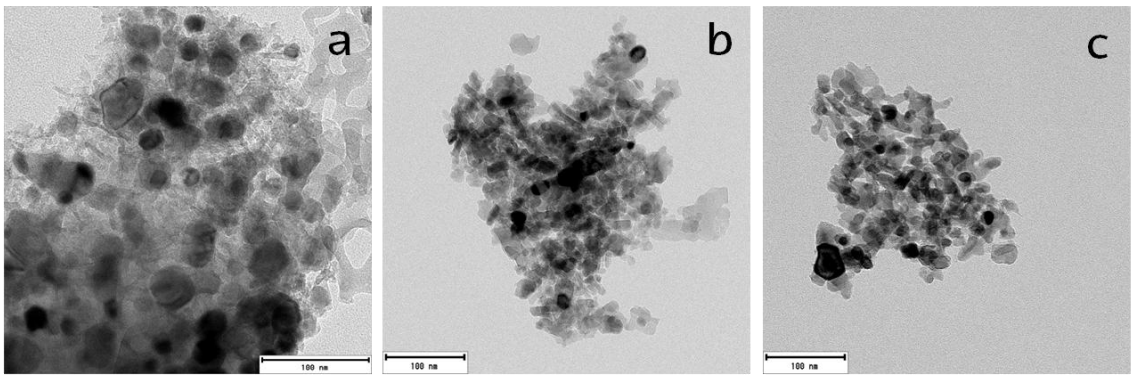

Figure 9. TEM images of the deactivated catalysts: G90LDP (a), Ni/Al_2O_3 (b) and Ni/La_2O_3-Al_2O_3 (c).

Once the performance of the catalyst and the mechanisms of its deactivation have been assessed, the regenerability of the different Ni based catalysts should be analyzed, since the recovery of catalyst activity and stability after regeneration is essential for the viability of scaling up this process. Accordingly, a previous research was carried out in order to determine the regenerability of the commercial G90-LPD catalyst used in this study [95]. It was concluded that, although catalyst activity was not fully recovered due to the irreversible deactivation by Ni sintering, the catalyst reached a pseudo-stable state beyond the fourth reaction-regeneration cycle, reproducing its behaviour in subsequent cycles.

Conclusions

The three catalysts studied are highly active for the reforming of biomass pyrolysis volatiles. The positive effect of La_2O_3 addition to the Ni/Al_2O_3 catalyst has been proven. Thus, it allows improving catalyst stability and achieving conversions higher than 97 %, with H_2 yields above 90 % for longer than 90 min on stream. Thus, the incorporation of La_2O_3 promoter attenuates catalyst deactivation rate, with this fact being attributed to the basic character of La_2O_3 promoter, which reduces the acidity of the support and inhibits the formation of coke. Moreover, its capability to favour water adsorption and dissociation leads to the gasification of the coke deposited and prevents catalyst deactivation. Consequently, the Ni/La_2O_3-Al_2O_3 catalyst has improved considerably the performance of the Ni/Al_2O_3 catalyst in terms of conversion, H_2 production, catalyst deactivation and stability.

However, coke deposition on the catalyst decreases H_2 and CO_2 yields and increases those of CO, CH_4, C_2-C_4 hydrocarbons and non-converted oxygenate compounds with time on stream. Although the Ni/La_2O_3-Al_2O_3 catalyst exhibited a high coke deposition amount after the reforming reaction due to its exposition to higher partial pressures of non-converted oxygenates compounds for more prolonged reaction times, the coke is not an evolved coke and burns at low temperatures.

Furthermore, the TPO profiles of deactivated catalysts show the lower temperature needed for the combustion of the coke on the Ni/La_2O_3-Al_2O_3 catalyst due to the properties of La_2O_3, which should be an advantage for the regeneration of the catalyst. The low combustion temperature is a consequence of the promotion of La_2O_3, which inhibits the evolution of the coke during the reforming reaction due to its basicity and water adsorption capacity. Consequently, high H_2 yields and productions have been obtained without operational problems, except those related to catalyst deactivation, which may be solved by regenerating the catalyst and operating with catalyst circulation in a fluidized bed reactor.

Acknowledgement

This work was carried out with financial support from the Spain's Ministry of Economy and Competitiveness (CTQ2016-75535-R (AEI/FEDER, UE), CTQ-2015-69436-R (MINECO/FEDER, UE) and RTI2018-101678-B-I00 (MCIU/AEI/FEDER, UE)), the Basque Government (IT1218-19), and from the European Union's Horizon 2020 research and innovation programme under the Marie Skłodowska-Curie grant agreement No 823745.

References

[1] Nikolaidis P, Poullikkas A. A comparative overview of hydrogen production processes. Renewable Sustainable Energy Rev. 2017;67:597-611. doi:10.1016/j.rser.2016.09.044.

[2] International Energy Agency (IEA) Technology roadmap: hydrogen and fuel cells. Paris, 2015.

[3] Pal DB, Chand R, Upadhyay SN, Mishra PK. Performance of water gas shift reaction catalysts: A review. Renewable Sustainable Energy Rev. 2018;93:549-65. doi:10.1016/j.rser.2018.05.003.

[4] Hosseini SE, Wahid MA. Hydrogen production from renewable and sustainable energy resources: Promising green energy carrier for clean development. Renewable Sustainable Energy Rev. 2016;57:850-66. doi:10.1016/j.rser.2015.12.112.

[5] Duman G, Yanik J. Two-step steam pyrolysis of biomass for hydrogen production. Int. J. Hydrogen Energy 2017;42:17000-8. doi:https://doi.org/10.1016/j.ijhydene.2017.05.227.

[6] Soria MA, Barros D, Madeira LM. Hydrogen production through steam reforming of bio-oils derived from biomass pyrolysis: Thermodynamic analysis including in situ CO2 and/or H2 separation. Fuel 2019;244:184-95. doi:https://doi.org/10.1016/j.fuel.2019.01.156.

[7] Nabgan W, Abdullah TAT, Mat R, Nabgan B, Gambo Y, Moghadamian K. Acetic acid-phenol steam reforming for hydrogen production: Effect of different composition of La2O3-Al2O3 support for bimetallic Ni-Co catalyst. J. Environ. Chem. Eng. 2016;4:2765-73. doi:10.1016/j.jece.2016.05.030.

[8] Resende KA, Ávila-Neto CN, Rabelo-Neto RC, Noronha FB, Hori CE. Hydrogen production by reforming of acetic acid using La-Ni type perovskites partially substituted with Sm and Pr. Catal. Today 2015;242:71-9. doi:10.1016/j.cattod.2014.07.013.

[9] Guan G, Kaewpanha M, Hao X, Abudula A. Catalytic steam reforming of biomass tar: Prospects and challenges. Renewable Sustainable Energy Rev. 2016;58:450-61. doi:10.1016/j.rser.2015.12.316.

[10] Ayalur Chattanathan S, Adhikari S, Abdoulmoumine N. A review on current status of hydrogen production from bio-oil. Renewable Sustainable Energy Rev. 2012;16:2366-72. doi:10.1016/j.rser.2012.01.051.

[11] Xue YP, Yan CF, Zhao XY, Huang SL, Guo CQ. Ni/La2O3-ZrO2 catalyst for hydrogen production from steam reforming of acetic acid as a model compound of bio-oil. Korean J. Chem. Eng. 2017;34:305-13. doi:10.1007/s11814-016-0277-1.

[12] Lopez G, Cortazar M, Alvarez J, Amutio M, Bilbao J, Olazar M. Assessment of a conical spouted with an enhanced fountain bed for biomass gasification. Fuel 2017;203:825-31. doi:10.1016/j.fuel.2017.05.014.

[13] Cortazar M, Lopez G, Alvarez J, Amutio M, Bilbao J, Olazar M. Behaviour of primary catalysts in the biomass steam gasification in a fountain confined spouted bed. Fuel 2019;253:1446-56. doi:https://doi.org/10.1016/j.fuel.2019.05.094.

[14] Liu L, Zhang Z, Das S, Kawi S. Reforming of tar from biomass gasification in a hybrid catalysis-plasma system: A review. Appl. Catal., B 2019;250:250-72. doi:https://doi.org/10.1016/j.apcatb.2019.03.039.

[15] Asadullah M. Biomass gasification gas cleaning for downstream applications: A comparative critical review. Renewable Sustainable Energy Rev. 2014;40:118-32. doi:10.1016/j.rser.2014.07.132.

[16] Abdoulmoumine N, Adhikari S, Kulkarni A, Chattanathan S. A review on biomass gasification syngas cleanup. Appl. Energy 2015;155:294-307. doi:10.1016/j.apenergy.2015.05.095.

[17] Alvarez J, Hooshdaran B, Cortazar M, Amutio M, Lopez G, Freire FB, Haghshenasfard M, Hosseini SH, Olazar M. Valorization of citrus wastes by fast pyrolysis in a conical spouted bed reactor. Fuel 2018;224:111-20. doi:https://doi.org/10.1016/j.fuel.2018.03.028.

[18] Yao D, Hu Q, Wang D, Yang H, Wu C, Wang X, Chen H. Hydrogen production from biomass gasification using biochar as a catalyst/support. Bioresour. Technol. 2016;216:159-64. doi:10.1016/j.biortech.2016.05.011.

[19] Chen F, Wu C, Dong L, Vassallo A, Williams PT, Huang J. Characteristics and catalytic properties of Ni/CaAlOx catalyst for hydrogen-enriched syngas production from pyrolysis-steam reforming of biomass sawdust. Appl. Catal., B 2016;183:168-75. doi:10.1016/j.apcatb.2015.10.028.

[20] Dong L, Wu C, Ling H, Shi J, Williams PT, Huang J. Promoting hydrogen production and minimizing catalyst deactivation from the pyrolysis-catalytic steam reforming of biomass on nanosized NiZnAlOx catalysts. Fuel 2017;188:610-20. doi:10.1016/j.fuel.2016.10.072.

[21] Jin F, Sun H, Wu C, Ling H, Jiang Y, Williams PT, Huang J. Effect of calcium addition on Mg-AlOx supported Ni catalysts for hydrogen production from pyrolysis-gasification of biomass. Catal. Today 2018. doi:10.1016/j.cattod.2018.01.004.

[22] Alvarez J, Kumagai S, Wu C, Yoshioka T, Bilbao J, Olazar M, Williams PT. Hydrogen production from biomass and plastic mixtures by pyrolysis-gasification. Int. J. Hydrogen Energy 2014;39:10883-91.

[23] Arregi A, Amutio M, Lopez G, Bilbao J, Olazar M. Evaluation of thermochemical routes for hydrogen production from biomass: A review. Energy Convers. Manage. 2018;165:696-719. doi:https://doi.org/10.1016/j.enconman.2018.03.089.

[24] Guan G, Chen G, Kasai Y, Lim EWC, Hao X, Kaewpanha M, Abuliti A, Fushimi C, Tsutsumi A. Catalytic steam reforming of biomass tar over iron- or nickel-based catalyst supported on calcined scallop shell. Appl. Catal., B 2012;115-116:159-68.

[25] Yang J, Kaewpanha M, Karnjanakom S, Guan G, Hao X, Abudula A. Steam reforming of biomass tar over calcined egg shell supported catalysts for hydrogen production. Int. J. Hydrogen Energy 2016;41:6699-705. doi:https://doi.org/10.1016/j.ijhydene.2016.03.056.

[26] Kumagai S, Alvarez J, Blanco PH, Wu C, Yoshioka T, Olazar M, Williams PT. Novel Ni-Mg-Al-Ca catalyst for enhanced hydrogen production for the pyrolysis-gasification of a biomass/plastic mixture. J. Anal. Appl. Pyrolysis 2015;113:15-21. doi:10.1016/j.jaap.2014.09.012.

[27] Cao JP, Ren J, Zhao XY, Wei XY, Takarada T. Effect of atmosphere on carbon deposition of Ni/Al2O3 and Ni-loaded on lignite char during reforming of toluene as a biomass tar model compound. Fuel 2018;217:515-21. doi:https://doi.org/10.1016/j.fuel.2017.12.121.

[28] Miyazawa T, Kimura T, Nishikawa J, Kado S, Kunimori K, Tomishige K. Catalytic performance of supported Ni catalysts in partial oxidation and steam reforming of tar derived from the pyrolysis of wood biomass. Catal. Today 2006;115:254-62. doi:https://doi.org/10.1016/j.cattod.2006.02.055.

[29] Li D, Ishikawa C, Koike M, Wang L, Nakagawa Y, Tomishige K. Production of renewable hydrogen by steam reforming of tar from biomass pyrolysis over supported Co catalysts. Int. J. Hydrogen Energy 2013;38:3572-81. doi:https://doi.org/10.1016/j.ijhydene.2013.01.057.

[30] Świerczyński D, Libs S, Courson C, Kiennemann A. Steam reforming of tar from a biomass gasification process over Ni/olivine catalyst using toluene as a model compound. Appl. Catal., B 2007;74:211-22. doi:https://doi.org/10.1016/j.apcatb.2007.01.017.

[31] Zhao XY, Ren J, Cao JP, Wei F, Zhu C, Fan X, Zhao YP, Wei XY. Catalytic Reforming of Volatiles from Biomass Pyrolysis for Hydrogen-Rich Gas Production over Limonite Ore. Energy Fuels 2017;31:4054-60. doi:10.1021/acs.energyfuels.7b00005.

[32] Zhao M, Church TL, Harris AT. SBA-15 supported Ni-Co bimetallic catalysts for enhanced hydrogen production during cellulose decomposition. Appl. Catal., B 2011;101:522-30. doi:https://doi.org/10.1016/j.apcatb.2010.10.024.

[33] Wu C, Wang L, Williams PT, Shi J, Huang J. Hydrogen production from biomass gasification with Ni/MCM-41 catalysts: Influence of Ni content. Appl. Catal., B 2011;108-109:6-13. doi:https://doi.org/10.1016/j.apcatb.2011.07.023.

[34] Wang BS, Cao JP, Zhao XY, Bian Y, Song C, Zhao YP, Fan X, Wei XY, Takarada T. Preparation of nickel-loaded on lignite char for catalytic gasification of biomass. Fuel Process. Technol. 2015;136:17-24. doi:https://doi.org/10.1016/j.fuproc.2014.07.024.

[35] Cao JP, Liu TL, Ren J, Zhao XY, Wu Y, Wang JX, Ren XY, Wei XY. Preparation and characterization of nickel loaded on resin char as tar reforming catalyst for biomass gasification. J. Anal. Appl. Pyrolysis 2017;127:82-90. doi:https://doi.org/10.1016/j.jaap.2017.08.020.

[36] Ren J, Cao JP, Zhao XY, Wei F, Liu TL, Fan X, Zhao YP, Wei XY. Preparation of high-dispersion Ni/C catalyst using modified lignite as carbon precursor for catalytic reforming of biomass volatiles. Fuel 2017;202:345-51. doi:https://doi.org/10.1016/j.fuel.2017.04.060.

[37] Ren J, Cao JP, Yang FL, Zhao XY, Tang W, Cui X, Chen Q, Wei XY. Layered uniformly delocalized electronic structure of carbon supported Ni catalyst for catalytic

reforming of toluene and biomass tar. Energy Convers. Manage. 2019;183:182-92. doi:https://doi.org/10.1016/j.enconman.2018.12.093.

[38] Yang FL, Cao JP, Zhao XY, Ren J, Tang W, Huang X, Feng XB, Zhao M., Cui X, Wei XY. Acid washed lignite char supported bimetallic Ni-Co catalyst for low temperature catalytic reforming of corncob derived volatiles. Energy Convers. Manage. 2019;196:1257-66. doi:https://doi.org/10.1016/j.enconman.2019.06.075.

[39] Ye M, Tao Y, Jin F, Ling H, Wu C, Williams PT, Huang J. Enhancing hydrogen production from the pyrolysis-gasification of biomass by size-confined Ni catalysts on acidic MCM-41 supports. Catal. Today 2016. doi:10.1016/j.cattod.2017.05.077.

[40] Waheed QMK, Wu C, Williams PT. Pyrolysis/reforming of rice husks with a Ni–dolomite catalyst: Influence of process conditions on syngas and hydrogen yield. J. Energy Inst. 2016;89:657-67. doi:10.1016/j.joei.2015.05.006.

[41] Efika CE, Wu C, Williams PT. Syngas production from pyrolysis-catalytic steam reforming of waste biomass in a continuous screw kiln reactor. J. Anal. Appl. Pyrolysis 2012;95:87-94.

[42] Cao JP, Shi P, Zhao XY, Wei XY, Takarada T. Catalytic reforming of volatiles and nitrogen compounds from sewage sludge pyrolysis to clean hydrogen and synthetic gas over a nickel catalyst. Fuel Process. Technol. 2014;123:34-40. doi:10.1016/j.fuproc.2014.01.042.

[43] Olaleye AK, Adedayo KJ, Wu C, Nahil MA, Wang M, Williams PT. Experimental study, dynamic modelling, validation and analysis of hydrogen production from biomass pyrolysis/gasification of biomass in a two-stage fixed bed reaction system. Fuel 2014;137:364-74. doi:10.1016/j.fuel.2014.07.076.

[44] Zou J, Yang H, Zeng Z, Wu C, Williams PT, Chen H. Hydrogen production from pyrolysis catalytic reforming of cellulose in the presence of K alkali metal. Int. J. Hydrogen Energy 2016. doi:10.1016/j.ijhydene.2016.04.207.

[45] Ren J, Cao JP, Zhao XY, Wei F, Zhu C, Wei XY. Extension of catalyst lifetime by doping of Ce in Ni-loaded acid-washed Shengli lignite char for biomass catalytic gasification. Catal. Sci. Technol. 2017;7:5741-9. doi:10.1039/c7cy01670k.

[46] Liu Y, Yu H, Liu J, Chen D. Catalytic characteristics of innovative Ni/slag catalysts for syngas production and tar removal from biomass pyrolysis. Int. J. Hydrogen Energy 2019;44:11848-60. doi:10.1016/j.ijhydene.2019.03.024.

[47] Garcia L, French R, Czernik S, Chornet E. Catalytic steam reforming of bio-oils for the production of hydrogen: Effects of catalyst composition. Appl. Catal., A 2000;201:225-39.

[48] Medrano JA, Oliva M, Ruiz J, García L, Arauzo J. Hydrogen from aqueous fraction of biomass pyrolysis liquids by catalytic steam reforming in fluidized bed. Energy 2011;36:2215-24. doi:10.1016/j.energy.2010.03.059.

[49] Santamaria L, Lopez G, Arregi A, Amutio M, Artetxe M, Bilbao J, Olazar M. Influence of the support on Ni catalysts performance in the in-line steam reforming of biomass fast pyrolysis derived volatiles. Appl. Catal., B 2018;229:105-13. doi:10.1016/j.apcatb.2018.02.003.

[50] Santamaria L, Lopez G, Arregi A, Amutio M, Artetxe M, Bilbao J, Olazar M. Stability of different Ni supported catalysts in the in-line steam reforming of biomass fast pyrolysis volatiles. Appl. Catal., B 2019;242:109-20. doi:10.1016/j.apcatb.2018.09.081.

[51] Santamaria L, Arregi A, Alvarez J, Artetxe M, Amutio M, Lopez G, Bilbao J, Olazar M. Performance of a Ni/ZrO2 catalyst in the steam reforming of the volatiles derived from biomass pyrolysis. J. Anal. Appl. Pyrolysis 2018;136:222-31. doi:10.1016/j.jaap.2018.09.025.

[52] Amutio M, Lopez G, Artetxe M, Elordi G, Olazar M, Bilbao J. Influence of temperature on biomass pyrolysis in a conical spouted bed reactor. Resour. Conserv. Recycl. 2012;59:23-31.

[53] Arregi A, Lopez G, Amutio M, Barbarias I, Bilbao J, Olazar M. Hydrogen production from biomass by continuous fast pyrolysis and in-line steam reforming. RSC Adv. 2016;6:25975-85. doi:10.1039/c6ra01657j.

[54] Cava S, Tebcherani SM, Souza IA, Pianaro SA, Paskocimas CA, Longo E, Varela JA. Structural characterization of phase transition of Al2O3 nanopowders obtained by polymeric precursor method. Mater. Chem. Phys. 2007;103:394-9. doi:https://doi.org/10.1016/j.matchemphys.2007.02.046.

[55] Wu YL, Hong J, Peterson D, Zhou J, Cho TS, Ruzic DN. Deposition of aluminum oxide by evaporative coating at atmospheric pressure (ECAP). Surf. Coat. Technol. 2013;237:369-78. doi:https://doi.org/10.1016/j.surfcoat.2013.06.043.

[56] Gauguin R, Graulier M, Papee D. Thermally stable carriers. Adv. Chem. Ser. 1975; 143:147-60.

[57] Baerns M. Basic principles in applied catalysis: Springer Ser. Chem. Phys., Berlin, Heidelberg, (2004).

[58] Arregi A, Amutio M, Lopez G, Artetxe M, Alvarez J, Bilbao J, Olazar M. Hydrogen-rich gas production by continuous pyrolysis and in-line catalytic reforming of pine wood waste and HDPE mixtures. Energy Convers. Manage. 2017;136:192-201. doi:http://dx.doi.org/10.1016/j.enconman.2017.01.008.

[59] Arregi A, Lopez G, Amutio M, Artetxe M, Barbarias I, Bilbao J, Olazar M. Role of operating conditions in the catalyst deactivation in the in-line steam reforming of volatiles from biomass fast pyrolysis. Fuel 2018;216:233-44. doi:https://doi.org/10.1016/j.fuel.2017.12.002.

[60] Barbarias I, Lopez G, Alvarez J, Artetxe M, Arregi A, Bilbao J, Olazar M. A sequential process for hydrogen production based on continuous HDPE fast pyrolysis

786 and in-line steam reforming. Chem. Eng. J. 2016;296:191-8.
787 doi:10.1016/j.cej.2016.03.091.

788 [61] Mazumder J, De Lasa HI. Ni catalysts for steam gasification of biomass: Effect of
789 La2O3 loading. Catal. Today 2014;237:100-10. doi:10.1016/j.cattod.2014.02.015.

790 [62] Osorio-Vargas P, Flores-González NA, Navarro RM, Fierro JLG, Campos CH,
791 Reyes P. Improved stability of Ni/Al2O3 catalysts by effect of promoters (La2O3,
792 CeO2) for ethanol steam-reforming reaction. Catal. Today 2016;259:27-38.
793 doi:10.1016/j.cattod.2015.04.037.

794 [63] Valle B, Remiro A, Aguayo AT, Bilbao J, Gayubo AG. Catalysts of Ni/α-Al2O3
795 and Ni/La2O3- αAl2O3 for hydrogen production by steam reforming of bio-oil aqueous
796 fraction with pyrolytic lignin retention. Int. J. Hydrogen Energy 2013;38:1307-18.
797 doi:10.1016/j.ijhydene.2012.11.014.

798 [64] Navarro RM, Guil-Lopez R, Ismail AA, Al-Sayari SA, Fierro JLG. Ni- and PtNi-
799 catalysts supported on Al2O3 for acetone steam reforming: Effect of the modification of
800 support with Ce, La and Mg. Catal. Today 2014. doi:10.1016/j.cattod.2014.07.036.

801 [65] Bereketidou OA, Goula MA. Biogas reforming for syngas production over nickel
802 supported on ceria-alumina catalysts. Catal. Today 2012;195:93-100.
803 doi:10.1016/j.cattod.2012.07.006.

804 [66] Charisiou ND, Siakavelas G, Papageridis KN, Baklavaridis A, Tzounis L, Avraam
805 DG, Goula MA. Syngas production via the biogas dry reforming reaction over nickel
806 supported on modified with CeO2 and/or La2O3 alumina catalysts. J. Nat. Gas Sci.
807 Eng. 2016;31:164-83. doi:10.1016/j.jngse.2016.02.021.

808 [67] Mustard DG, Bartholomew CH. Determination of metal crystallite size and
809 morphology in supported nickel catalysts. J. Catal. 1981;67:186-206. doi:10.1016/0021-
810 9517(81)90271-2.

811 [68] Garcia-Garcia I, Acha E, Bizkarra K, Martinez De Ilarduya J, Requies J, Cambra
812 JF. Hydrogen production by steam reforming of m-cresol, a bio-oil model compound,
813 using catalysts supported on conventional and unconventional supports. Int. J.
814 Hydrogen Energy 2015;40:14445-55. doi:10.1016/j.ijhydene.2015.07.155.

815 [69] Valle B, Aramburu B, Remiro A, Bilbao J, Gayubo AG. Effect of
816 calcination/reduction conditions of Ni/La2O3-aAl2O3 catalyst on its activity and
817 stability for hydrogen production by steam reforming of raw bio-oil/ethanol. Appl.
818 Catal., B 2014;147:402-10. doi:10.1016/j.apcatb.2013.09.022.

819 [70] International Centre for Diffraction Data. 2003.

820 [71] Tilley RD, Jefferson DA. The preparation of chromium, nickel and chromium-
821 nickel alloy nanoparticles on supports. J. Mater. Chem. 2002;12:3809-13.
822 doi:10.1039/b204774h.

[72] Wang M, Zhang F, Wang S. Effect of La2O3 replacement on G-Al2O3 supported nickel catalysts for acetic acid steam reforming. Int. J. Hydrogen Energy 2017;42:20540-8. doi:10.1016/j.ijhydene.2017.06.147.

[73] Bizkarra K, Bermudez JM, Arcelus-Arrillaga P, Barrio VL, Cambra JF, Millan M. Nickel based monometallic and bimetallic catalysts for synthetic and real bio-oil steam reforming. Int. J. Hydrogen Energy 2018. doi:10.1016/j.ijhydene.2018.03.049.

[74] Yamamoto T, Hatsui T, Matsuyama T, Tanaka T, Funabiki T. Structures and Acid-Base Properties of La/Al2O3 - Role of La Addition to Enhance Thermal Stability of γ-Al2O 3. Chem. Mater. 2003;15:4830-40. doi:10.1021/cm034732c.

[75] Bettman M, Chase RE, Otto K. , Weber WH. Dispersion studies on the system La2O3 γ-Al2O3. J. Catal. 1989;117:447-54. doi:10.1016/0021-9517(89)90354-0.

[76] Mekhemer GAH, Ismail HM. Dispersion of ceria and lanthana on silica and alumina supports - X-ray diffractometry and nitrogen sorptometry studies. Colloids Surf., A 2004;235:129-36. doi:10.1016/j.colsurfa.2003.12.009.

[77] Ibrahim HH, Idem RO. Single and mixed oxide-supported nickel catalysts for the catalytic partial oxidation reforming of gasoline. Energy Fuels 2008;22:878-91. doi:10.1021/ef7005904.

[78] Mellin P, Kantarelis E, Zhou C, Yang W. Simulation of bed dynamics and primary products from fast pyrolysis of biomass: Steam compared to nitrogen as a fluidizing agent. Ind. Eng. Chem. Res. 2014;53:12129-42. doi:10.1021/ie501996v.

[79] Choong CKS, Huang L, Zhong Z, Lin J, Hong L. , Chen L. Effect of calcium addition on catalytic ethanol steam reforming of Ni/Al2O3: II. Acidity/basicity, water adsorption and catalytic activity. Appl. Catal., A 2011;407:155-62. doi:10.1016/j.apcata.2011.08.038.

[80] Salehi E, Azad FS, Harding T, Abedi J. Production of hydrogen by steam reforming of bio-oil over Ni/Al2O3 catalysts: Effect of addition of promoter and preparation procedure. Fuel Process. Technol. 2011;92:2203-10. doi:10.1016/j.fuproc.2011.07.002.

[81] Liu S, Chen M, Chu L, Yang Z, Zhu C, Wang J, Chen M. Catalytic steam reforming of bio-oil aqueous fraction for hydrogen production over Ni-Mo supported on modified sepiolite catalysts. Int. J. Hydrogen Energy 2013;38:3948-55. doi:10.1016/j.ijhydene.2013.01.117.

[82] Arandia A, Coronado I, Remiro A, Gayubo AG, Reinikainen M. Aqueous-phase reforming of bio-oil aqueous fraction over nickel-based catalysts. Int. J. Hydrogen Energy 2019;44:13157-68. doi:https://doi.org/10.1016/j.ijhydene.2019.04.007.

[83] Valle B, Aramburu B, Olazar M, Bilbao J, Gayubo AG. Steam reforming of raw bio-oil over Ni/La2O3-αAl2O3: Influence of temperature on product yields and catalyst deactivation. Fuel 2018;216:463-74. doi:10.1016/j.fuel.2017.11.149.

[84] Zhang Y, Li W, Zhang S, Xu Q, Yan Y. Steam reforming of bio-oil for hydrogen production: Effect of Ni-Co bimetallic catalysts. Chem. Eng. Technol. 2012;35:302-8. doi:10.1002/ceat.201100301.

[85] Bimbela F, Oliva M, Ruiz J, García L, Arauzo J. Hydrogen production via catalytic steam reforming of the aqueous fraction of bio-oil using nickel-based coprecipitated catalysts. Int. J. Hydrogen Energy 2013;38:14476-87. doi:10.1016/j.ijhydene.2013.09.038.

[86] Fu P, Yi W, Li Z, Bai X, Zhang A, Li Y, Li Z. Investigation on hydrogen production by catalytic steam reforming of maize stalk fast pyrolysis bio-oil. Int. J. Hydrogen Energy 2014;39:13962-71. doi:10.1016/j.ijhydene.2014.06.165.

[87] Ochoa A, Arregi A, Amutio M, Gayubo AG, Olazar M, Bilbao J. , Castaño P. Coking and sintering progress of a Ni supported catalyst in the steam reforming of biomass pyrolysis volatiles. Appl. Catal., B 2018;233:289-300. doi:10.1016/j.apcatb.2018.04.002.

[88] Waheed QMK, Williams PT. Hydrogen production from high temperature pyrolysis/steam reforming of waste biomass: Rice husk, sugar cane bagasse, and wheat straw. Energy Fuels 2013;27:6695-704. doi:10.1021/ef401145w.

[89] Chen J, Sun J, Wang Y. Catalysts for Steam Reforming of Bio-oil: A Review. Ind. Eng. Chem. Res. 2017;56:4627-37. doi:10.1021/acs.iecr.7b00600.

[90] Montero C, Ochoa A, Castaño P, Bilbao J, Gayubo AG. Monitoring Ni0 and coke evolution during the deactivation of a Ni/La2O3-αAl2O3 catalyst in ethanol steam reforming in a fluidized bed. J. Catal. 2015;331:181-92. doi:10.1016/j.jcat.2015.08.005.

[91] Ochoa A, Aramburu B, Valle B, Resasco DE, Bilbao J, Gayubo AG, Castaño P. Role of oxygenates and effect of operating conditions in the deactivation of a Ni supported catalyst during the steam reforming of bio-oil. Green Chem. 2017;19:4315-33. doi:10.1039/c7gc01432e.

[92] Zhang F, Wang M, Zhu L, Wang S, Zhou J, Luo Z. A comparative research on the catalytic activity of La2O3 and G-Al2O3 supported catalysts for acetic acid steam reforming. Int. J. Hydrogen Energy 2017;42:3667-75. doi:10.1016/j.ijhydene.2016.06.264.

[93] Remiro A, Arandia A, Oar-Arteta L, Bilbao J, Gayubo AG. Regeneration of NiAl2O4 spinel type catalysts used in the reforming of raw bio-oil. Appl. Catal., B 2018;237:353-65. doi:10.1016/j.apcatb.2018.06.005.

[94] Sánchez-Sánchez MC, Navarro RM, Fierro JLG. Ethanol steam reforming over Ni/La-Al2O3 catalysts: Influence of lanthanum loading. Catal. Today 2007;129:336-45. doi:10.1016/j.cattod.2006.10.013.

[95] Arregi A, Lopez G, Amutio M, Barbarias I, Santamaria L, Bilbao J, Olazar M. Regenerability of a Ni catalyst in the catalytic steam reforming of biomass pyrolysis volatiles. J. Ind. Eng. Chem. 2018;68:69-78. doi:10.1016/j.jiec.2018.07.030.

Figure1

Click here to download high resolution image

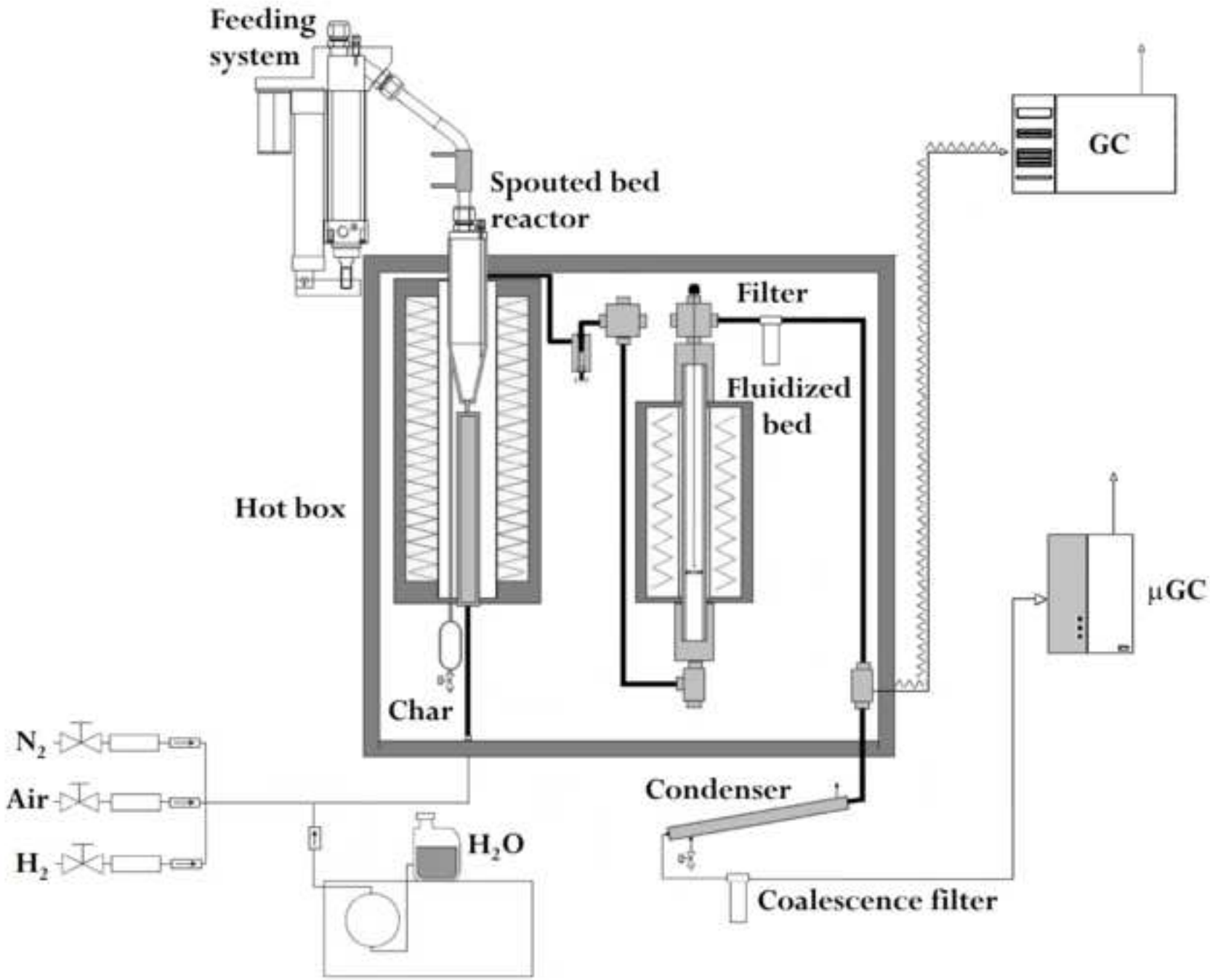

Figure2
Click here to download high resolution image

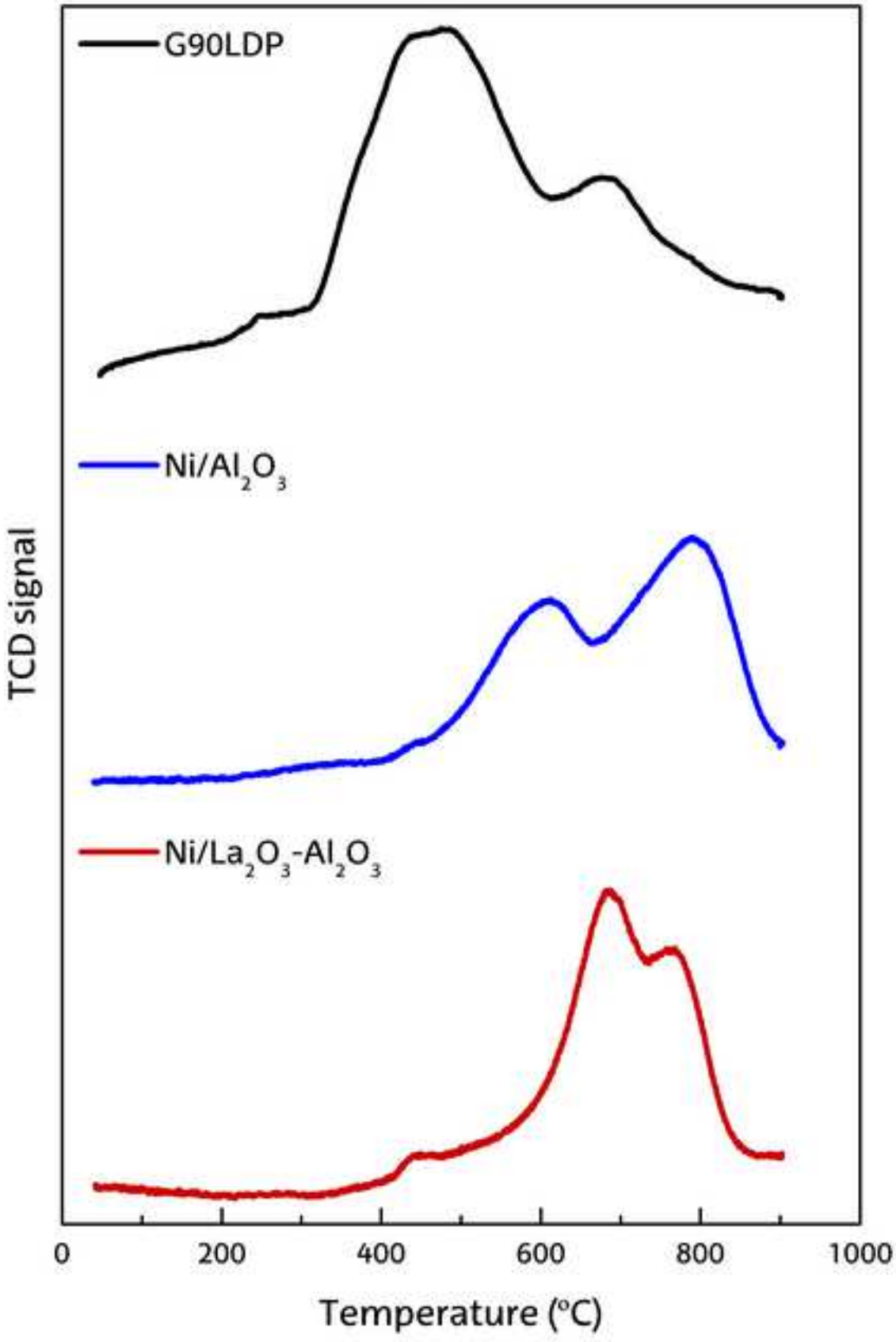

Figure3

Click here to download high resolution image

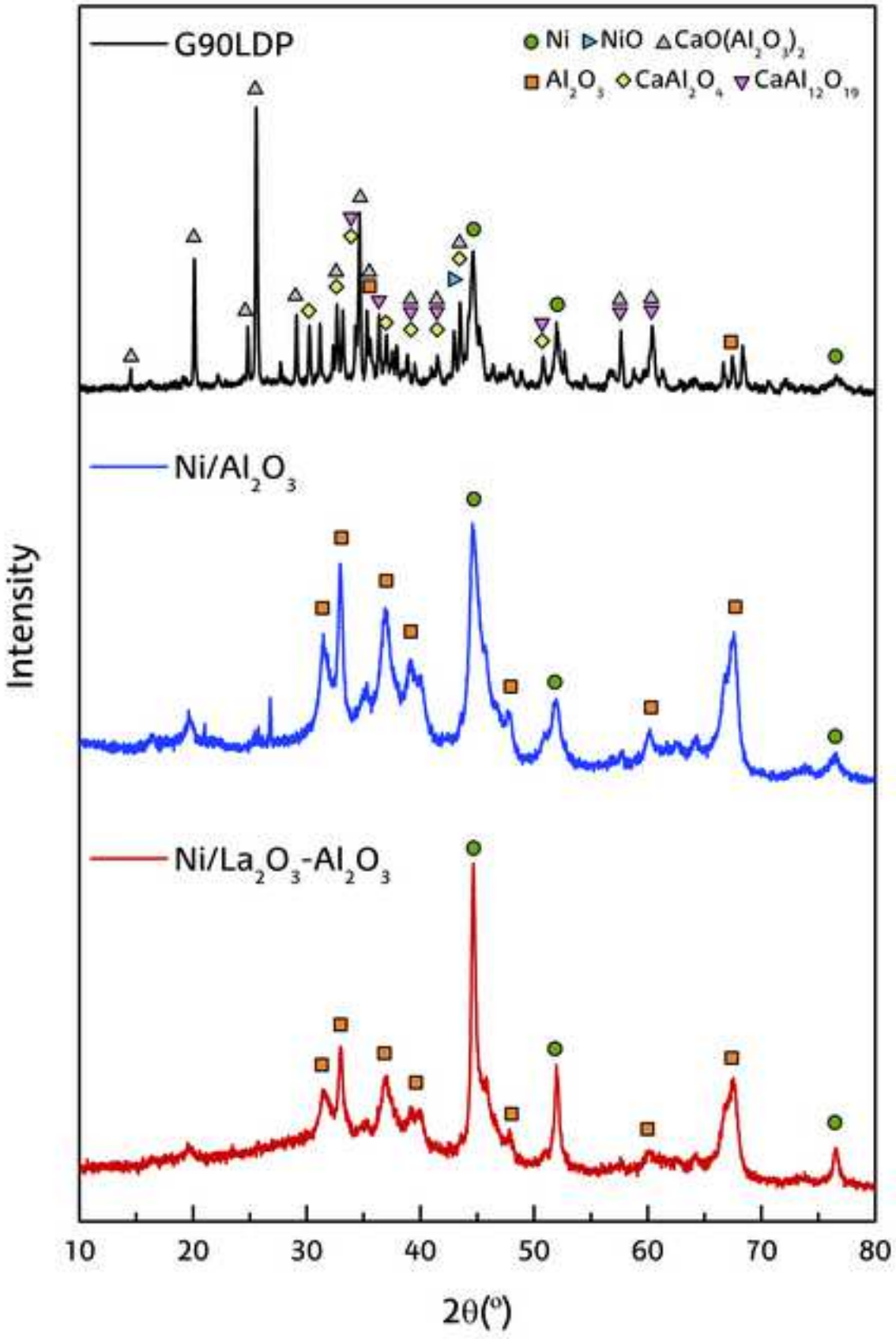

Figure4
Click here to download high resolution image

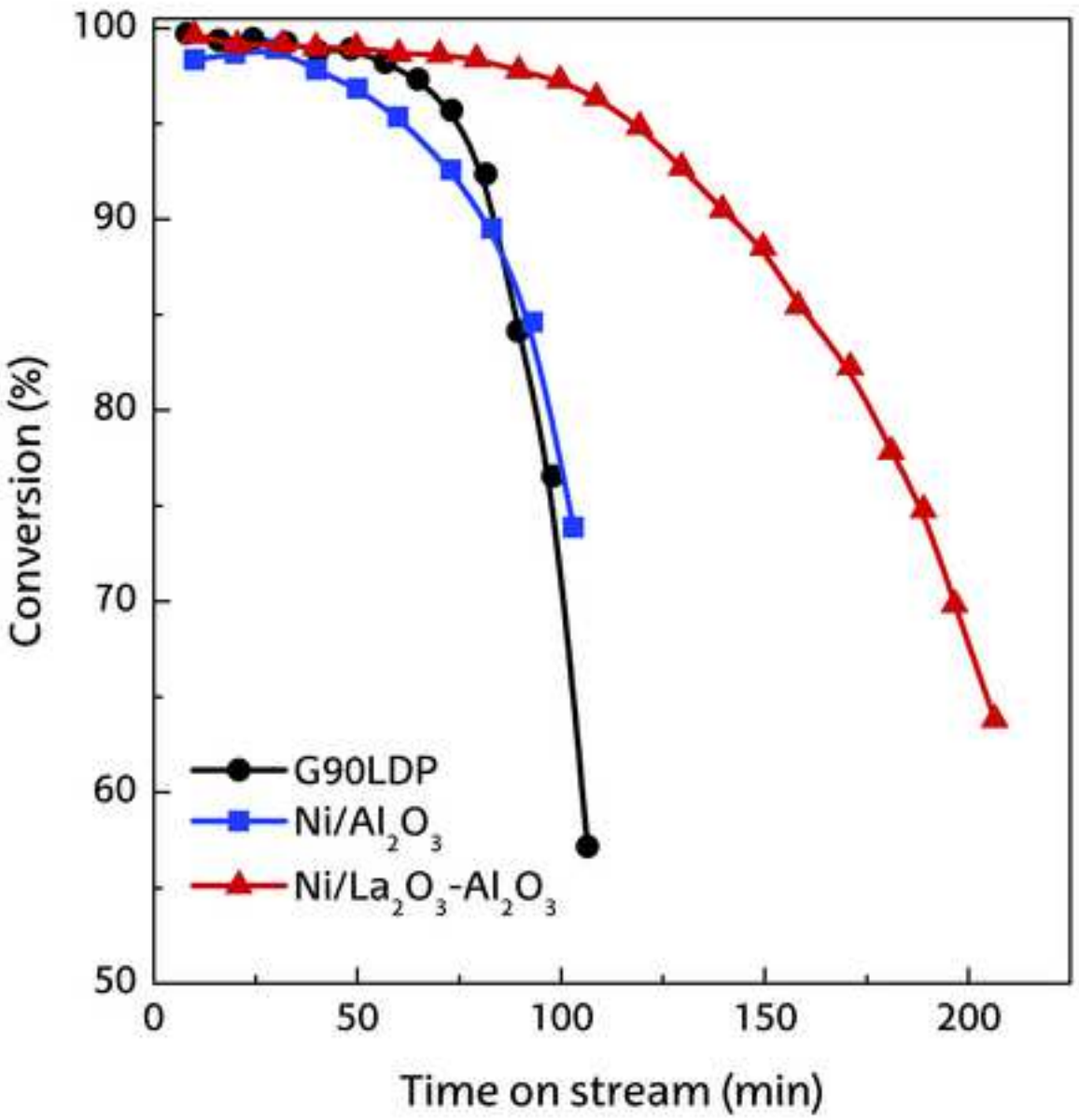

Figure5

Click here to download high resolution image

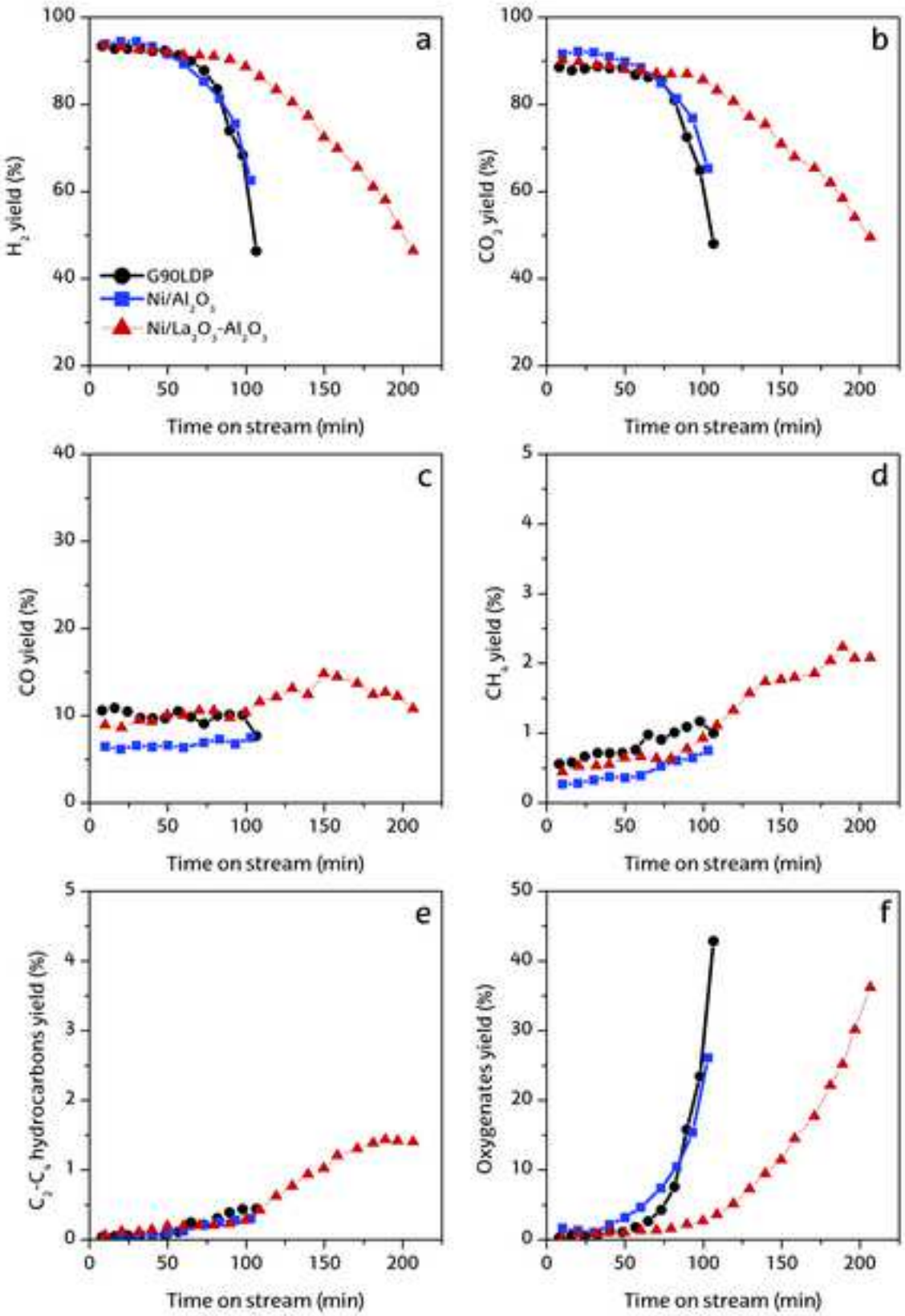

Figure6
Click here to download high resolution image

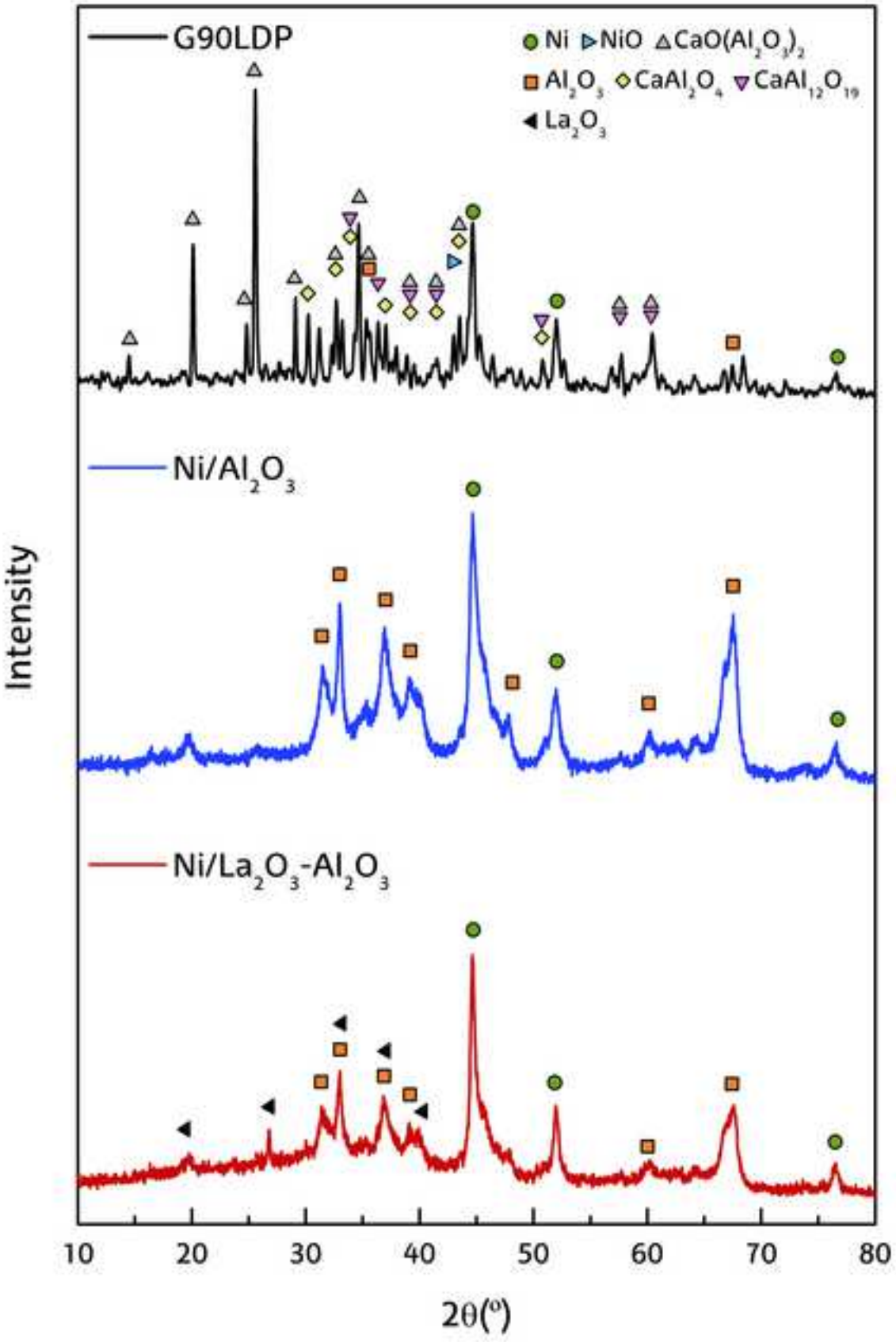

Figure7
Click here to download high resolution image

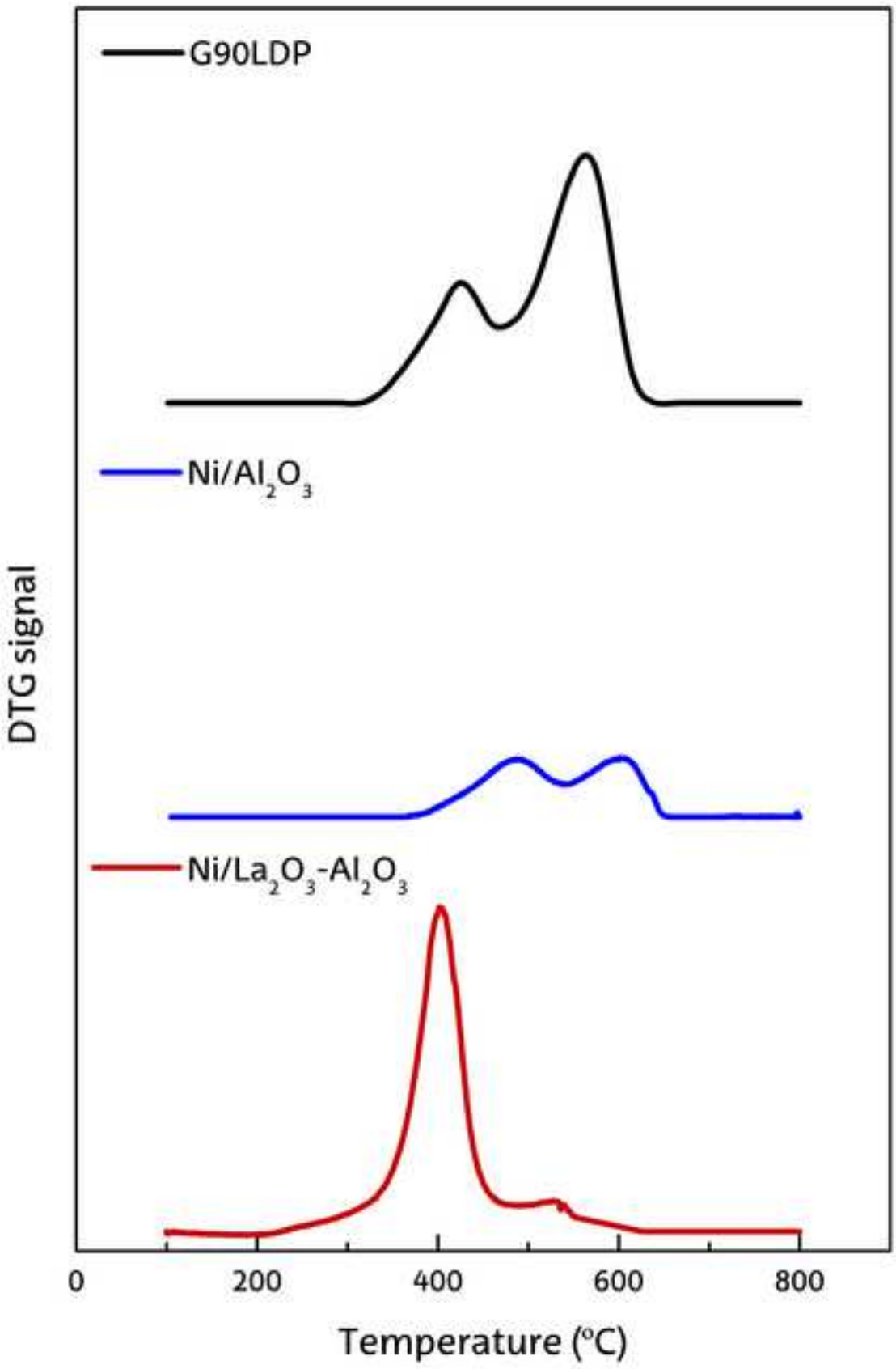

Figure8

Click here to download high resolution image

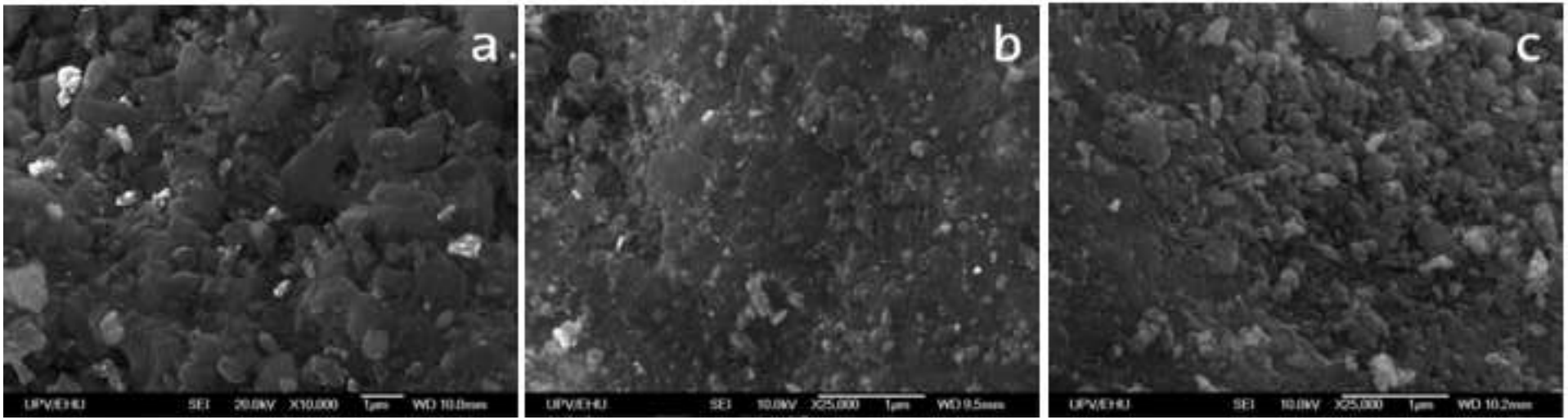

Figure9
Click here to download high resolution image

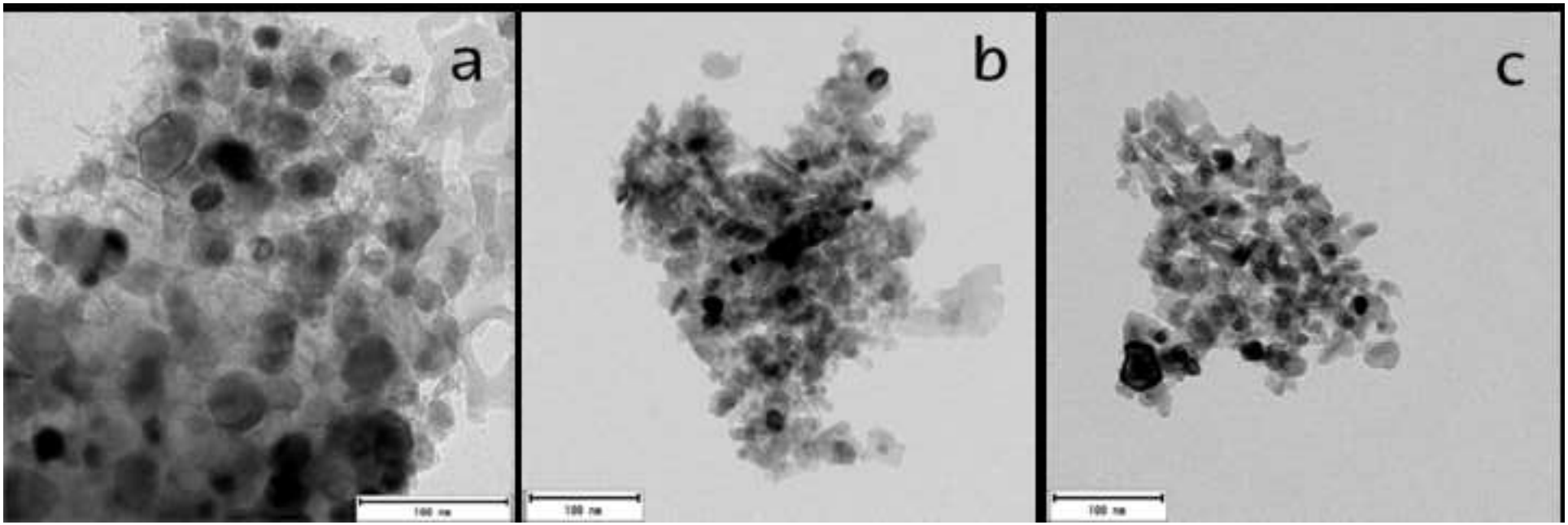

***Declaration of Interest Statement**

Declaration of interests

■ The authors declare that they have no known competing financial interests or personal relationships that could have appeared to influence the work reported in this paper.

☐The authors declare the following financial interests/personal relationships which may be considered as potential competing interests: